AUTHOR(S):

TITLE:

YEAR:

Publisher citation:

OpenAIR citation:

Diametral compression test method to analyse relative surface stresses in thermally sprayed coated and uncoated circular disc specimens

N.H. Faisal[a],[1], L. Mann[a], C. Duncan[a], E. Dunbar[a], M. Clayton[a], M. Frost[a], J. McConnachie[a], A. Fardan[b], R. Ahmed[b]

[a] *School of Engineering, Robert Gordon University, Garthdee Road, Aberdeen, AB10 7GJ, UK*

[b] *School of Engineering and Physical Sciences, Heriot-Watt University, Edinburgh, EH14 4AS, UK*

Abstract

In firsts of its investigation, a diametral compression destructive testing method (also known as Brazilian test) was performed on thermally sprayed coated and uncoated circular disc specimens to compare relative surface stresses. The coating investigated had about 250 µm thickness deposited on 4.76 mm thick Hastelloy®X substrate discs of 20 mm diameter. In the instrumented experiment (diametral compression test) strain gauge rosettes were used to measure strains on two circular surfaces of disc specimen (coated and uncoated sides) and converted to stress values for analysis. Where comparisons were made, the experimental and finite element simulation results were in some agreement with overall understanding of the diametral compression testing behaviour. For coated specimen, test results convey that higher stresses exist within the uncoated side of the specimen rather than the coated side. Although the methods proposed would be deemed most comparable to real life scenarios (e.g. to quantify coating delamination strength and failure mechanics), this type of experimental investigation has certain advantages and limitations.

Keywords: diametral compression test; Brazilian test; thermal spray coatings; strain gauge, residual stress; analytical method; finite element.

---

[1] Corresponding authors. E-mail addresses: N.H.Faisal@rgu.ac.uk; Tel: +44 (0) 1224-26 2438.

1. Introduction

Normally, Hertzian contact mechanics models are used to determine the change in the contact area of a surface as loads are exerted on a contacting surface. This process can also be applied during the compression test of a specimen to all occurrences of material contact. Hertzian contact mechanics theory is one of the earlier developments in contact theory [1], which is limited to the following assumptions: (a) the material surfaces in contact are continuous and are different nonconforming surfaces, (b) the contact surfaces are frictionless, and (c) only small strains are valid - as too large strains would cause the material to become plastic rather than elastic. Both solids are treated as having an elastic half space, the depth of the deformation due to the loading would not cause plastic deformation on either material [2].

Brazilian testing is a methodology of compression testing where the contacting surface on the cylinder specimen (or disc in current study) is either curved and rigid or flat and rigid as can be illustrated in **Fig. 1(a)**. The Brazilian disc test has been introduced as a convenient substitute of the direct tensile test in the case of brittle materials (mainly rock like ones and concrete) [3-4]. Also shown in **Fig. 1(b)** an isotropic disc section (two-dimensional) in compression with two rigid plate being the contact surface, where R is the original radius, a is the contact radius, δ is the deformation, and P is the force applied to the disc. Hertzian pressure theory predicts, for a diametral compression test of a disk, that the largest magnitude of principal stress is located at the centre of the disk. It also predicts that the stress is tensile in the x-direction and compressive in y-direction. Tensile strength (σ_f) of a disc in contact with a flat surface can be found from Hertz theory by the following relationship;

$$\sigma_f = \frac{P}{\pi R t} = \frac{2P}{\pi D t} \qquad (1)$$

where R is the radius (or diameter, D) of the circular specimen that is in contact with the plate and t is thickness of the disc. Brazilian testing methodology can be used for brittle materials and ceramics as was performed by Scapin *et al.* (2017) [5] in finding the tensile strength of

alumina. This testing is well documented where it is mostly used to find strength and deformation of rock discs as was performed by Chen *et al.* (1998) [6].

Huang *et al.* (2012) [7] set out to determine the bond strength within a composite concentric disc focusing on stress distribution through finite element (FE) method. The composite concentric disc consisted of glass fibre post, dentin and resin. It is subjected to compression from a steel block. Other relevant work was carried out by Furukawa *et al.* (2015) [8] who sought out to determine an effective method for evaluating the capping tendency during a diametral compression test of pharmaceutical tablets (microcrystalline cellulose) using FE. Experimental work by Procopio *et al.* (2003) [9] found that this relationship is accurate for linear elastic materials of which are brittle and will fracture. This is validated through FE and referred to as the stress at the centre of the circular specimen by Es-Saheb *et al.* (2011) [10] of whom also describes empirical formula for the stresses at any point on the disk. FE study performed by Sahoo and Chatterjee (2010) [11] found that for an elastic-perfectly plastic material in contact with a rigid surface that the elastic modulus to yield stress ratio (E/σ_y) effects contact behaviour. If the ratio is less than 300, which this causes parameters including the hardness and contact pressure to not be constant in the contacting surface but are constant if the ratio is above 300.

Several models and theories have been developed from Hertz's original work to analytically model contact more accurately with less broad assumptions. This can be possible due to several effects being neglected by Hertzian theory. Interfacial friction is an influence if the two materials in contact (the specimen and the test machine) have different elastic constants. Resisting this friction at the edges of the surface slip occurs and will always take place if the materials are different. Adhesion is a phenomenon not considered in Hertz theory which occurs at the middle of the contacting surface and requires a force to overcome it often referred to as the pull off force. This influences the contact area after the compression has taken place and refers to the Johnson, Kendall and Roberts (JKR) theory of elasticity [2].

Standard compression testing (ASTM E9-09) [12] standardises compressive testing of metallic materials, which includes recommended equipment and specifications of the specimens. The main failure documented from the test of the specimen is crushing due to the compression test, but the standard also highlights other methods of failure during this test such as non-axial loading causing lack of elastic instability or the occurrence of inelastic instability or torsional instability.

Considering thermal spray coating formation, residual strain (or stresses) are formed within the coating and substrates due to many processes (quenching stress, peening effect, deposition temperature, lamella structure) and phase differences [13-18]. However, traditionally, as presented by Godoy *et al.* [19], residual stresses mainly arise from two different sources: (a) shrinkage of the spray particles after solidification (primary cooling process), and (b) differences between the coating and substrate thermal expansion coefficients (secondary cooling process). Also summarised by Araujo *et al.* [20], during the first stage of deposition, individual molten particles heat the substrate leading to solidification. Since complete contraction is not possible (owing to the presence of the substrate and/or the neighbouring particles), which leads to residual stresses, called 'quenching stresses'. The second stage of the spraying process is related to the cooling of the coating. The presence of the 'cooling stresses' is due to both the mismatch between the thermal expansion coefficients and the temperature difference between the coating and the substrate. State-of-the-art schematic representation of stresses (quenching, cooling), leading to residual stresses has been well documented by Pina *et al.* [21]. However, depending on the spraying process (e.g. air plasma, high velocity oxy-fuel, etc.) as presented by Sampath *et al.* [22], or as a function of temperature of deposition as presented by Matejicek *et al.* [23], the distribution, intensity and sign of the residual stresses can be very different through thickness (i.e. tensile, compressive or combination of tensile and compressive). Luo, Selvadurai and Tillman [24] concluded that the thickness of coating and substrate geometry can modify the residual stress (i.e. absolute

residual stress increases with the thickness of the coating). The compressive stresses induced by thermal spray coating has a significant positive influence on the wear resistance, whereas the tensile stress has a negative effect. The compressive stress can prevent the initiation and propagation of the cracks [25]. However, tensile stress can lead to delamination by cracking or loss of adhesion. Better adhesion between a coating and its substrate is expected when the mean residual stresses in the region of the interface are as low as possible [26-30].

Measurement of stresses is therefore important to evaluate coating quality (e.g. adhesion, fatigue, tribological behaviour). Non-destructive (laboratory X-ray, synchrotron X-ray, neutron, Raman spectroscopy, digital image correlation, photoluminescence piezospectroscopy), semi-destructive (hole-drilling & ring-coring, layer removal, focused ion beam milling, indentation), and miscellaneous other (curvature, modified layer removal, material removal) approaches have been adapted to experimentally evaluate the residual stress fields in thermal spray coatings. The measured values of stress in the coating-substrate system can be sensitive to the stress measurement technique, which in turn can influence the predicted life of coated components [13-18]. However, this study will consider a diametral compression destructive testing method on thermally sprayed and uncoated circular disc specimens to compare the surface relative stresses.

The first objective of this study is to evaluate the strain and stress distributions of the thermally sprayed coated circular disc and uncoated circular disc under diametral compression, and to understand how the coated disc affect and address variations in stress distribution. The second objective is to explain the sequence of events observed during the test, i.e. from elastic to interfacial failure leading to final coating delamination from the disc substrate. For these reasons, we used the strain gauge based instrumented diametral compression method, then finite element method to measure strains (or stress), and finally the analytical method. It is expected that the methods presented in this investigation will stimulate efforts towards measuring coating delamination strength and change in structural strength.

The following section on the theoretical aspect of diametral compression testing method (Brazilian test) was necessary as this is firsts investigation of its kind on thermally sprayed coated and uncoated circular disc specimens to compare relative surface stresses.

2. Theory

2.1 Stresses in a circular disc

This section presents a theory related to stresses in a circular disc during diametral compression test. The following section applies this theory to a coated circular disc. As derived by Johnson (1985) [2], the elastic compression of two-dimensional disc (for isotropic material) in contact cannot be calculated solely from the contact stresses given by the Hertz theory. The compression of a disc which is in non-conformal contact with two other surfaces along two generators located at opposite ends of a diameter can be analysed satisfactorily. As shown in **Fig. 1(c)**, the compressive load (P) per unit axial length gives rise to a Hertzian distribution of pressure (p) at O_1:

$$p = \frac{2P}{\pi a}\left(1 - \frac{x^2}{a^2}\right)^{1/2} \qquad (2)$$

where the semi-contact width, a (assuming contact width is same on both side of the vertical axis, y) is given by:

$$a^2 = \frac{4PR}{\pi E_i^*} \qquad (3)$$

where E_i^* can be found from composite modulus equation ($\frac{1}{E_i^*} = \frac{1-\nu_1^2}{E_1} + \frac{1-\nu^2}{E}$) of the compressing plate and the disc, R is radius of the disc, and ν_1 and ν are Poisson's ratio of non-conformal compressing plates and disc, respectively. The stress distribution (Timoshenko and Goodier, 1951 [31]) in a disc due to diametrically opposed concentrated loads comprises the

stress fields due to two concentrated forces (P) acting at O_1 and O_2, together with a uniform bi-axial tension (**Fig. 1(c)**):

$$\sigma_x = \sigma_y = \frac{P}{\pi R} \tag{4}$$

Since $a \ll R$, we can consider the disc as being subjected to a combination of diametrically opposed forces distributed according to Equation (2). The stress at point A is made up of three contributions: (i) the stress due to Hertzian distribution of pressure on the contact at O_1, given by Equation (2), (ii) the stress due to the contact pressure at O_2, which, in view of the large distance of A from O_2, can be taken to be that due to a concentrated force, P, and (iii) the bi-axial tension given by Equation (4). Therefore, the stresses at A (**Fig. 1(c)**):

$$\sigma_x = \frac{P}{\pi}\left\{\frac{1}{R} - \frac{2\left(a^2 + 2y^2\right)}{a^2\left(a^2 + y^2\right)^{1/2}} + \frac{4y}{a^2}\right\} \tag{5a}$$

$$\sigma_y = \frac{P}{\pi}\left\{\frac{1}{R} - \frac{2}{2R - y} - \frac{2}{\left(a^2 + y^2\right)^{1/2}}\right\} \tag{5b}$$

In plane strain,

$$\varepsilon_y = \left(\frac{1-v^2}{E}\right)\left\{\sigma_y - \sigma_x\left(\frac{v}{1-v}\right)\right\} \tag{6}$$

The compression of the upper half of the disc (O_1C) is then found by integrating ε_y from $y = 0$ to $y = R$, where $a \ll R$, to give

$$\delta_1 = P\left(\frac{1-v^2}{\pi E}\right)\left\{2\ln\left(\frac{4R}{a}\right) - 1\right\} \tag{7}$$

Therefore, the total compression of the diameter (assuming contact width a is same on both sides of the vertical axis, y, and assume that the disc does not tilt) through the mid-points of the contact areas (O_1O_2) is

$$\delta = 2\delta_1 \tag{8}$$

The compression of a half-space relative to a point at a depth d below the centre of a Hertzian contact pressure distribution can be,

$$\delta = P\left(\frac{1-v^2}{\pi E}\right)\left\{2\ln\left(\frac{2d}{a}\right)-\frac{v}{(1-v)}\right\} \qquad (9)$$

As presented by Johnson (1985) [2], taking $d = R$, the true compression of the half-disc (Equation (7)) exceeds the compression based upon a half-space (Equation (9)) by less than 10% within the practical range of loads.

2.2 Stresses in a coated circular disc

This section presents a theory related to stresses in a coated circular disc (coating on one flat side of the disc) during diametral compression test. As shown in **Fig. 2(a,b)**, the disc under investigation can be considered as composite (coating-substrate) disc of same radius (R) and perfectly bonded at interface of different thicknesses (t_c as coating thickness; t_s as substrate thickness). The elastic modulus and Poisson's ratio can be considered for coating as (E_c, v_c) and for substrate as (E_s, v_s).

Therefore, based on theory discussed above, the elastic compression of two-dimensional composite disc (coating-substrate system) in non-conformal contact with two other surfaces along two generators located at opposite ends of a diameter can also be analysed satisfactorily. The stress distribution (σ_{xc}, σ_{yc} : coating; σ_{xs}, σ_{ys} : substrate) in a composite disc due to diametrically opposed concentrated loads comprises the superposition of the stress fields (of two half-spaces within coating and substrate system) due to two concentrated forces (P) acting at O_1 and O_2 (**Fig. 1(c)**), together with a uniform bi-axial tension (assuming strain in the coating and substrate is equal as the change in dimension of both will be the same under the assumption of perfect bonding and two concentrated forces, P):

$$\sigma_{xc} = \sigma_{yc} = \frac{P}{\pi R} \qquad (10a)$$

$$\sigma_{xs} = \sigma_{ys} = \frac{P}{\pi R} \qquad (10b)$$

Similarly, the stresses at A (consider coated specimen, **Fig. 1(c)**):

$$\sigma_{xc} = \frac{P}{\pi}\left\{\frac{1}{R} - \frac{2(a^2 + 2y^2)}{a^2(a^2 + y^2)^{1/2}} + \frac{4y}{a^2}\right\} \qquad (11a)$$

$$\sigma_{yc} = \frac{P}{\pi}\left\{\frac{1}{R} - \frac{2}{2R - y} - \frac{2}{(a^2 + y^2)^{1/2}}\right\} \qquad (11b)$$

And the stresses at A (consider in substrate of coated specimen, **Fig. 1(c)**):

$$\sigma_{xs} = \frac{P}{\pi}\left\{\frac{1}{R} - \frac{2(a^2 + 2y^2)}{a^2(a^2 + y^2)^{1/2}} + \frac{4y}{a^2}\right\} \qquad (12a)$$

$$\sigma_{ys} = \frac{P}{\pi}\left\{\frac{1}{R} - \frac{2}{2R - y} - \frac{2}{(a^2 + y^2)^{1/2}}\right\} \qquad (12b)$$

In plane strain (consider coated specimen, **Fig. 1(c)**),

$$\varepsilon_{yc} = \left(\frac{1 - v_c^2}{E_c}\right)\left\{\sigma_{yc} - \sigma_{xc}\left(\frac{v_c}{1 - v_c}\right)\right\} \qquad (13a)$$

$$\varepsilon_{ys} = \left(\frac{1 - v_s^2}{E_s}\right)\left\{\sigma_{ys} - \sigma_{xs}\left(\frac{v_s}{1 - v_s}\right)\right\} \qquad (13b)$$

The compression of the upper half of each disc (coating, substrate) is then found by

integrating ε_{yc} and ε_{ys} from $y = 0$ to $y = R$, where $a << R$, to give

$$\delta_{1c} = P\left(\frac{1 - v_c^2}{\pi E_c}\right)\left\{2\ln\left(\frac{4R}{a}\right) - 1\right\} \qquad (14a)$$

$$\delta_{1s} = P\left(\frac{1 - v_s^2}{\pi E_s}\right)\left\{2\ln\left(\frac{4R}{a}\right) - 1\right\} \qquad (14b)$$

Therefore, the total compression of the diameter (assuming contact width a is same on both side of the vertical axis, y, and assume that the composite disc does not tilt) through the mid-points of the contact areas (O_1O_2) is

$$\delta = 2\delta_{1c} = 2\delta_{1s} \qquad\qquad (15)$$

The mismatch in compression (for example when $2\delta_{1c} < 2\delta_{1s}$), can lead to coating delamination due to shear strain at the coating-substrate interface.

3. Materials and methods

3.1 Coating and disc substrate materials

The coated disc specimen was sourced from work completed previous to the investigation [13, 32], as shown in **Fig. 3(a)**. The disc substrate of 20 mm diameter and 4.76 mm thick used in the investigation was Hastelloy®X, provided by Haynes International Limited, Manchester, UK. For the coating (about 250 µm thickness) under investigation a combination of molybdenum carbide (Mo-Mo$_2$C), powder catalyst and a metal oxide powder (i.e. Al$_2$O$_3$) were used. The powder was used to create feedstock powder which allowed for the fabrication of coated specimen (i.e. Mo-Mo$_2$C/Al$_2$O$_3$, with a stoichiometric ratio of 0.8:0.2). Air plasma spray (APS) deposition was carried out at an industrial thermal spray facility (Monitor Coating Limited, UK), using a spray system.

As per the scheme shown in **Fig. 4** (inbox) [13], nanoindentation trials for elastic modulus (at 30 mN load, instrument chamber temperature 300 K) of the coating and substrate cross-sections were performed using a calibrated NanoTest™ system (Micromaterials Limited, UK) with a diamond Berkovich tip. The elastic modulus (E_i) and Poisson's ratio (ν_i) of the diamond indenter were taken as 1140 GPa and 0.07, respectively, whereas, to calculate the elastic modulus (E_s) of the specimen, the Poisson ratio for the coated layer (ν_c) was assumed as 0.30 (Molybdenum Poisson's ratio) and for the substrate (ν_s) was presumed

to be 0.32 [33]. Where necessary for substrate, the stresses were then normalised by dividing by the theoretical yield stress (385 MPa) of Hastelloy®X [34].

3.2 Test sample preparation and strain gauge location

The strain increment measured by a strain gauge is only proportional to the elastic strain when perfectly elastic material behaviour can be assumed at the measurement location. Plastic deformation of material makes it impossible to relate measured strain values to other stresses (e.g. residual stress). For the bare disc specimen and for the uncoated sides of the coated specimen, the surface was prepared for strain gauge assembly (**Fig. 3(b)**). To have increased bond strength, 320 grit sandpaper was used as an abrasive to increase the contact surface area of the face of the specimen with the bonding agent (Loctite® Super Glue Precision). The bonding glue for strain gauge assembly was let to cure in ambient laboratory conditions. Alcohol (isopropanol) was used to decontaminate the surface of the material. The remaining alcohol was then dabbed dry to ensure all residues were removed before adhesion. Due to the way in which the coated specimens were sprayed, coating residue was present around the edges of the disc (**Fig. 3(a)**). This coating will absorb some of the stresses intended to be exerted on the substrate-coating system therefore it was removed using 320 grit sandpaper.

3.3 Strain gauge instrumentation

As a compressive load was exerted on the specimen, it was known that a tensile strain would be induced at 90° to the direction of the compressional strain. This was of interest therefore bi-element strain gauges (circuit being a quarter bridge with two-wire connection as the cable length was shorter) were used during testing, measuring these two changes of strain with load. For the strain experiment carried out, stacked rosette general purpose strain gauges were used for the test (stacked rosette KFG-2-D17-11L 30, Kyowa Electronic Instruments),

with 2.0 mm gauge length and 5% strain limit at room temperature. Strain gauges provides the results directly as strains and not as the change in the strain gauge resistance during testing. Strain relief is an important factor to consider when applying strain gauges. Low magnitude stress (for example, the weight of the wires) upon a stress concentrated section of the lead wire may result in fracture. Therefore, thin plastic films were glued on top of the components to relief some of the stress exerted, after the glue set, excess plastic was removed. Wires were soldered to the strain gauge ribbon leads and connected to the CompactRIO, where results were recorded via LabVIEW^{TM}.

The National Instruments CompactRIO (cRIO) programmable automation controller was used to receive the signals created by the strain gauges. The RIO architecture, which contains a real-time processor, a reconfigurable Field Programmable Gate Array (FPGA), and swappable I/O modules, was connected. For the experiment carried out, CompactRIO scan mode was used. Scan mode allowed the user to programme the real-time processor of the CompactRIO but not the FPGA. In this mode, National Instrument^{TM} provide the programming for the FPGA based on scanning the I/O modules and placing it into a memory map, making it available to LabVIEW^{TM} Real-Time module. The virtual instrument (VI) for the experiment carried out contains the readings from the 120 V quarter bridges programmed into the CompactRIO channels connected to graphical indicator in order to display the results. The entire VI was created in a timed-loop with a sampling rate of 10 Hz to give ten strain readings a second. A limitation of this VI set-up was that the VI could not log the data independently, therefore, only what was witnessed in the graphs could be exported to excel. A maximum of 1023 data plots along the x-axis was selected, giving a maximum timeframe of approximately 100 seconds before data loss occurred. Each experiment was thus timed during loading and to ensure no data loss occurred, experiments were stopped after 90 seconds of loading.

3.4 Diametral compression (static Brazilian test) loading

To verify the analytical solutions (*Section 2*), a series of diametral compression tests were carried out. The Instron®3382 universal testing machine (loading capacity: 100 kN) was utilised to apply a compressive load to the specimens (shown in **Fig. 3(b)**). In this experimental procedure, only the upper compression plate is moving (downwards) and therefore the displacements along y-axis are not symmetric with respect to the horizontal x-axis of symmetry. The Instron®3382 loading machine was operated by Bluehill® software where a rate and direction of displacement can be established for the test. All the samples were tested at a loading rate of 2 mm/min. This loading rate selection was made based on some trial runs. For uncoated Hastelloy®X substrates, a strain rate of 1 mm/min was initially applied, and this test was stopped at around 1.5 mm displacement. The maximum displacement was appropriate as yielding of the Hastelloy®X was observed before this maximum value was reached. During trial runs, for the coated samples, a strain rate of 1 mm/min was tested, however, the coating did not fail (inspected visually). Therefore, the strain rate was varied to 2 mm/min which successfully fractured (and/or delaminated) the coatings (Mo-Mo_2C/Al_2O_3 on Hastelloy®X substrate) in the given timeframe.

During strain gauge data capture, a variation in resistance is observed even in the absence of external loadings, considered as a noise which was recorded for a minute before testing occurred. This noise was time-averaged and subtracted from the results obtained in the VI to filter out the noise received by the instrumentation, which was completed for all the test specimens. It was acknowledged that the complex geometry of the specimen lead to a complex analysis, due to Hertzian contact. However, assumptions were made to greatly simplify this. A pure bi-axial analysis was completed during the investigation, meaning that Poisson's ratio across the *z*-axis was ignored. An assumption was made when calculating stress field at the surface of disc centre (to use Hooke's law for stress values, it is necessary to ensure that strain gauge locations do not undergo plastic deformation), as the strain measured

was multiplied by the elastic modulus at the surface of the coating or substrate found by previous work on the same coating-substrate systems [13]. It is acknowledged that the elastic modulus of the substrate varies slightly with the coating applied [13], as shown in **Fig. 4** (with average elastic modulus value of 205±82 GPa for coating).

Practice testing was completed to develop the technique over numerous tests to create a robust method. It was acknowledged prior to testing that slippage might occur, therefore a notched plastic jig (**Fig. 3(b)**) was created to load the specimen so that the applied load would be uniaxial upon the specimen. As Bluehill® software live displayed the load-displacement curve, the jig would be removed once an acceptable load was reached (around 5 kN) knowing that this would not move the specimen. It is possible the test specimen can be loaded off-axis – leading to inaccuracies within the testing (a direct application of compressive force, free from eccentricity, can be difficult, and little could be done to fix any off-axial loading).

It is understood that during compression loading (as the external load increases) both compression plates and the specimen are gradually deformed (either plastically or elastically) and the contact is realised along a finite arc of the cross section symmetric with respect to both axis [4]. Although the compression plates are usually considered as an ideally rigid body in many practical applications, the disc and compression plates relative deformability (quantified by the ratio of their elastic moduli) cannot be ignored [4], but usually the gradual change of the contact length is ignored.

3.5 Finite element modelling of diametral compression loading

The stress within the coating and substrate material was analysed using a commercially available finite element software (ABAQUS, v.6.16). A three-dimensional elastic-plastic contact stress model was developed to mimic the experimental loading of the disc substrate with the coating. The geometry of the coated specimen was modelled with two

compressive plates in the top and bottom in contact with the coated substrate to replicate the experimental test (**Fig. 5**).

The input parameters for the simulation of the disc substrate and the coating are given in **Fig. 2**. The yield stress of the Hastelloy-X$^{®}$ substrate is taken as 385 MPa [34] and for Mo-Mo$_2$C/Al$_2$O$_3$ it is assumed as 770 MPa (at zero plastic strain). The experimental value of the yield stress of Mo-Mo$_2$C/Al$_2$O$_3$ coating material was not evaluated and an approximation was made based on the difference in hardness values of the coating-substrate system, since there can be a linear relation between the hardness and yield strength [35-36]. The yield stress of the coating based on the hardness of the coating was roughly twice of the Hastelloy-X$^{®}$ substrate [13]. The following assumptions were made in the finite element simulations: (a) materials were isotropic, homogeneous and linear elastic, (b) contact between the compressive plate and the specimen occur along a line, and (c) perfect bonding between the coating and the substrate. The bottom end of the lower plate was fixed, while the upper plate was given a displacement of $\delta = 1.6$ mm in the Y-direction and the disc was restricted translational motion in X- and Z-directions, for which the boundary condition was applied on the uncoated surface and this boundary condition was deactivated during the simulation to mimic the experiment. The element type used in ABAQUS is hexahedral (C3D8R, a general purpose linear brick element) for the substrate, coating and the plate. Mesh convergence was carried out for the coated disc until a point at which the maximum von-Mises stress did not vary. The converged model consisted of 28,392 elements for the substrate and 2366 elements for the coating. Surface-to-surface contact was specified in the interaction module of ABAQUS and coefficient of friction value of 0.2 was applied to the points where the upper and lower compression plates are in contact with the substrate. The tie-adjust constraint was used to model the interaction between the coating and substrate.

A simple finite element model allows to study the quantitative influence of the model dimension and properties. The implementation of some real specimen conditions (e.g. elastic

modulus, phase composition, microstructure of the individual coating and the substrate, load stresses, residual stresses, interface geometry, mechanical boundary conditions, microcracks, influence of layers, etc.) may not be straight forward in modelling. Although a more realistic simulations [e.g. 37-42] (beyond the scope of current work) can yield valuable insights into the effect of the microstructure on stresses or crack propagation.

4. Results and discussion

4.1 Standalone disc substrate

As obtained from the strain gauges, typical data, are shown in **Fig. 6(a)** regarding the distribution of the ε_x and ε_y components of the displacement field at the centre of the specimen's surface for a load level about 20 kN. The test as shown in **Fig. 6(a)** was first completed using uncoated Hastelloy®X specimens to develop a working procedure for the coated specimens. The results allowed for a comparison to be made later between the coating and substrate. **Figure 6** convey the effects that loading had on standalone uncoated substrate. From this figure, it is made evident that the load-displacement graphs are non-linear. Usually for a simple square/rectangular plate specimen this would be deemed incorrect, however as the specimen is circular disc, this is expected.

Diametric compression induces an indirect tensile test which is at maximum perpendicular to the loading direction and is proportional in magnitude to the applied load [10]. When the graphs are observed more closely, suggesting that linearity does not always seem to occur almost to the point of yield (where $\frac{\sigma}{\sigma_y} = 1$, **Fig. 6(b)**)) before a curve becomes much more evident. The $\sigma_y = 385 MPa$ (yield strength at 0.2% offset, for sheet 2.3 mm to 7.9 mm thick at room temperature) value used for Hastelloy®X is obtained via theoretical value [34]. The stresses upon the centre of the specimen may be still be in the elastic limits however influenced by the Hertzian contact which occurred with load, or by the central zone on the

surface reaching yield stress. As shown through vertical and horizontal red lines at the point

of yield (**Fig. 6(b)** and then coordinates traced in **Fig. 6(a)**), the *y*-axis strains and stresses are

offset (higher) by about 110 µm compared to *x*-axis strains and stresses. As per the theory

presented in *Section 2.1*, the comparison of *x*-axis and *y*-axis stresses in uncoated circular disc

will be presented in later section.

4.2 Comparison of coated to uncoated disc faces

During testing of the coated specimens, strain gauges were attached to both the coated

and uncoated faces of the specimen (at the centre) to gain an understanding of the differences

in stress experienced between the substrate and thermal sprayed coating surfaces during the

loading process. **Figure 7(a,b)** displays the strains and stresses in the *x*- and *y*-directions for

the coated specimen. **Figure 7(c)** displays the normalised stresses for the uncoated face of the

coated specimen (using $\sigma_y = 385 MPa$ for Hastelloy®X), again suggesting that linearity in the

x- and *y*-directions does not always seem to occur almost to the point of yield (where $\dfrac{\sigma}{\sigma_y} = 1$)

before a curve becomes much more evident.

As shown through vertical and horizontal red lines at the point of yield (**Fig. 7(c)** and

then traced in **Fig. 7(a,b)**), the coordinates are symmetric (*y*-axis strains and stresses are same

compared to *x*-axis strains and stresses in uncoated faces of the specimen, respectively),

indicating symmetricity between two directions, with slight asymmetric coordinates for the

coated side. Up to the point of yield, the stresses upon the centre of the specimen (coated side

and through thickness in coating) may be still be in the elastic limits, however, stresses upon

the centre of the specimen (uncoated side and through thickness in substrate) may be in the

plastic deformation zone, leading to initiation in coating delamination due to mis-match in

stresses at the coating-substrate interface. For coated specimen, the uncoated face experiences

more strain and thus more stress than the coated side.

As observed through recent investigation ([13], ***Appendix A.1***), neutron diffraction residual stress values for the same coating-substrate specimen (Mo-Mo$_2$C/Al$_2$O$_3$ coating on Hastelloy$^®$X substrate), it was observed that the difference between average residual stress (102 MPa in substrate, 41 MPa in substrate) is about 61 MPa, with about 150 MPa average stress mis-match at the interface. It can be observed that the through thickness residual strain (or stress) profile is complex and ideally it could be superimposed on the compression stress field [13]. However, such experimental data of residual strain (or stress) is not three dimensional and such superimpositions is not trivial for a three-dimensional stress field during the compression test. The failure of the coating in the current study is detachment or delamination at the coating substrate interface. The residual stress profile at the coating substrate interface (***Appendix A.1***) shows low stress in the coating and a compressive stress at the coating-substrate interface. However, in the current example, the compressive residual strain (or stress) could be helpful in combating the delamination failure at the interface [21-24].

Scanning electron microscopy (SEM) images of the coated surface have been provided (**Fig. 8(a)**). As presented for Mo-Mo$_2$C/Al$_2$O$_3$ coating surface, the coating is porous – interconnected voids (in specimen cross-section, **Fig. 8(b)**). Strains influenced by the diametral compression test will have great difficulty spanning across the coating as the strains will become more localised across the coating splats in comparison to the solid homogenous Hastelloy$^®$X substrate. However, the difference in stress or strain values (i.e. the point of yield between coating and substrate in the *x*-axis and *y*-axis directions at the centre of the specimen are shown in **Fig. 7(b)**) is about 226 MPa in tensile direction and about 285 MPa in compressive direction. These values are higher than average stress mis-match at the interface of about 150 MPa using neutron diffraction method [13]. The stress values (from current diametral compression test) which could possibly initiate coating to delaminate from the substrate. Therefore, the proposed diametral compression test method may be an alternative to

ASTM C633 ("Standard Test Method for Adhesion or Cohesion Strength of Thermal Spray Coatings") [43], to quantify the initiation of adhesion failure (or adhesion strength) at the centre of the specimen.

4.3 Comparison between coated and uncoated (bare) disc specimen

Figure 9 illustrate the strain, stress and normalised stresses with loading of the Mo-Mo$_2$C/Al$_2$O$_3$ coated disc specimen and comparison with bare Hastelloy®X substrate. The initiation of cracking (or delamination) is first made obvious by a reduction in stress across the *y*-axis of the coating. The fracture is then made evident in **Fig. 9(a,b)** at 1.5 mm displacement as the stress shoots up, this is not actually due to an increase in stress along the *x*-axis but displays an open circuit due to the fracture of the strain gauge. This was caused by a fracture (or delamination) in the coating along the axis of loading. This kind of fracture is expected in a brittle material and similar cracking from the same kind of experiment [44] where it was shown the fracture of barre granite from diametric compression. Although this cracking was expected and well-known, the causes of this fracture is argued. At first it was assumed that the induced nominal tensile stresses previously discussed was the cause of fracture, however it has been proven that the fracture is initiated from the load points. It has been presented by Sampath *et al.* (1986) [45] using a 300 µm gold film crack gauge that a plastic flow occurs before the fracture, making the material first reach plasticity at the loading contact before the plastic region is extended to the centre of the specimen. The fracture thus initiates at the centre of the disk from an intensified tensile stress in this location [45].

Figure 9(c) compares the normalised stresses for the uncoated face of the coated specimen (using $\sigma_y = 385 MPa$ for Hastelloy®X) against bare disc specimens, again suggesting that linearity in the *x*- and *y*-directions does not always seem to occur almost to the point of yield (where $\frac{\sigma}{\sigma_y} = 1$) before a curve becomes much more evident. As shown through

vertical and horizontal red lines at the point of yield (**Fig. 9(c)**), indicating that coating can enhance the yield strength of the disc substrate.

4.4 Coating delamination behaviour under diametral compression loading

A presence of through thickness pre-existing residual stress field in a coating-substrate system can strongly affect the coatings failure in the presence of induced load stresses. Considering the superposition of induced load stresses and coating process induced residual stresses, it is important to note that there is no simple relationship between coating delamination (cracking) pattern and total stress distribution during diametral compression loading, but diametral compression loading stress and pre-existing residual stress can affect the coating failure behaviour significantly. As shown in **Fig. 10**, significant coating cracking leading to interfacial delamination has occurred during diametral compression loading. The reason this phenomenon has occurred is suspected to be due to a mismatch of strain between the substrate/coating interface and external compression loading.

As mentioned in *Section 4.2*, because of their complex nature, including properties which vary with coating depth and multi-phase mixture of materials of varying toughness, published work on the effect of through-thickness residual stress their mechanical response is limited, and this investigation provides insight to their adhesive behaviour and failure mechanisms [21-24]. In some of the important work, models developed by Clyne and Gill [26] presented mathematical formulations of residual stresses in thermal spray coatings and their effects on interfacial delamination, whereas, Tsui and Clyne model [46] can be used to predict the residual stress distributions in progressively deposited coatings. It is important to note that Tsui and Clyne model [46] is based on the concept of a misfit strain, caused by either the deposition stress (e.g. due to quenching of splats in thermal spraying) or by differential thermal contraction between substrate and coating during cooling. The deposition stress is introduced as the coating is formed layer-by-layer, such that the misfit strain is

accommodated after each layer addition (rather than for the coating as a whole). Meanwhile, as presented by Godoy *et al.* [19], considering an imposed misfit strain in the interface planar direction, such as would arise during a change in temperature, the resultant stress distribution and curvature properties can be obtained from simple beam bending theory. Godoy *et al.* [19] also outlined the effect of the shear (relevant due to compression loading in current work) and peeling stress for evaluating the coating/substrate adhesion.

Rough surface (high shear zone) and smooth surface (low shear zone) can be observed in **Fig. 10(b)**. Such variation in surface roughness on the substrate surface is possible as the substrate at the interface is subjected to a greater stress than that of the coating at the interface for the same level of displacement, thus creating a stress concentration. **Figure 10(b)** suggest what appears to be Hertzian contact stress lobes at the points of contact. This also highlights the area where elements could yield on the shear failure developed along the centre of the coated specimen.

4.5 Finite element analysis of diametral compression loading

The maximum von-Mises stress acting on the substrate is 385 MPa while for the coating is 770 MPa (**Fig. 11**). The von-Mises stress acting on the substrate and coating is limited to their respective yield stresses since the stress was defined for zero plastic strain. It is to be noted that the substrate undergoes flattening on the surfaces interacting with the compressive plates (shown in **Fig. 11(a)**), like the experimental behaviour (shown in **Fig. 10(b)**). The maximum XY shear stress on the substrate is 190 MPa and for the coating is 418 MPa (**Fig. 12**). It is seen that the shear stress has both tensile and compressive stresses of equal magnitude acting around the point of contact which is expected in a Hertzian contact analysis.

The evolution of the stresses in the *x*- and *y*-direction at the centre of the Hastelloy-X® substrate and Mo-Mo_2C/Al_2O_3 coating is shown in **Fig. 13** (for elastic-plastic in **Fig. 13(a)**,

for perfectly elastic model in **Fig. 13(b)**). For the elastic-plastic model it is seen at a displacement value of about 0.9 mm, the coating and the substrate reaches the yield stress while from the experimental results, the yield is reached for a displacement value of 1.2 mm (shown in **Fig. 7**). The stress values displayed for the perfectly elastic model is displayed up to a displacement of 0.9 mm, since the ABAQUS model terminates due to high deformation for the perfectly elastic model. The stresses obtained for the perfectly elastic model is higher than the elastic-plastic model since there is no yield stress defined and when compared with experimental results, the elastic-plastic results are in better agreement than perfectly elastic model.

The study of the interfacial stresses between the coating and substrate is carried out by measuring the stresses along the paths as shown in **Fig. 14**. The von-Mises stress along the *y*-axis and *x*-axis for the coating have been depicted in (**Fig. 15**), the maximum von-Mises stress for the coating and substrate is 770 MPa and 385 MPa, respectively. It is seen that the stress along the distance is constant since the whole disc and substrate reaches the yield stress for displacement of 1.6 mm.

The XY shear stress acting on the substrate and coating (for left and right orientations, **Fig. 12 (c,d)**) are plotted in **Fig. 16**. It is seen that the compressive and tensile stresses of equal magnitude are present. The maximum XY shear stress for the coating is found to be 350 MPa, while for the substrate is 150 MPa. The shaded regions under the curves in **Fig. 15** and **Fig. 16** depicts the mismatch of stress between the coating and substrate which causes the coating delamination (shown in **Fig. 10(b)**). The stress acting on the coating is higher than the substrate around the point of contact which causes the coating to delaminate. Comparing the variation of stress with displacement for the elastic-plastic model and the experiment, the behaviour is similar, but the stress values do not match. This is due to the various assumptions taken into consideration for the FE model such as elastic-perfectly plastic, and the perfect bonding between the coating and substrate, which is not true in the case of experiment. For

more accurate results, the FE model must incorporate the bond strength for the coating and substrate while including plasticity (with stresses for various plastic strain values) in the model and to use cohesive behaviour between the coating and the substrate to study the delamination strength. It has also been demonstrated that it is not straightforward to estimate the behaviour of cracks from a micromechanical stress simulation [37] because the formation and propagation of microcracks changes the stress state significantly. Importantly, if the interest is more in understanding the main features of stress evolution during compression loading than in performing quantitatively accurate calculations, a simple finite element simulation is advantageous.

4.6 Analytical stress interpretation

As presented in *Section 2.1*, the analytical model related to stresses in a circular disc during diametral compression test has been summarised in detail in previous work (Johnson, 1985 [2]). However, analytical interpretation of similar model for a composite circular disc coated on one side of the flat surface may be useful in quantifying the stresses (σ_x, σ_y) at each material disc centre (at $y = R$) (**Fig. 17**, example calculations shown in ***Appendix A.2***).

As shown through vertical red line at the point of yield (refer **Fig. 7(c)** and then traced in **Fig. 17(a)**), and from the results of the analytical equations (*Section 2.2*, Eq. 10(a,b)), it was found that the stresses (bi-axial *x*- and *y*-direction stresses using $\sigma_x = \sigma_y = \dfrac{P}{\pi R}$, **Fig. 17(a)**) will have significant mismatch at the interface. Similarly, from the results of the analytical equations (*Section 2.2*, Eq. 11(a,b) and Eq. 12(a,b)), it was found that the stresses

(*x*-direction stresses using $\sigma_x = \dfrac{P}{\pi}\left\{\dfrac{1}{R} - \dfrac{2(a^2 + 2y^2)}{a^2(a^2 + y^2)^{1/2}} + \dfrac{4y}{a^2}\right\}$, and *y*-direction stresses using

$$\sigma_y = \frac{P}{\pi} \left\{ \frac{1}{R} - \frac{2}{2R - y} - \frac{2}{\left(a^2 + y^2\right)^{1/2}} \right\}$$, **Fig. 17(b,c)**) will have significant mismatch at the

interface.

From above analysis, it is anticipated that the analytical modelling has certain limitation (i.e. experimental and FE stress profiles are very different if compared to analytical stress profiles) and development of appropriate model can be part of further work. Overall, despite some experimental and theoretical limitations, the proposed diametral compression loading methodology on thermally sprayed coating-substrate systems presents a good summary of the novel findings.

5. Conclusions

In first of its investigation, the proposed diametral compression test method (i.e. Brazilian disc) was somewhat successful in the stress analysis of a thermal sprayed coating/substrate system. In this method strain gauge rosettes are pasted, respectively, at the centre on the both side faces of disc (along the direction and perpendicular to the compression line load) which are used to record tensile and compression strain of the centre part. Based on the results (experimental, simulation and analytical methods), we present the following concluding remarks for the diametral compression test of thermal spray coated disc substrate:

a. For coated disc specimen, experimental test results convey that higher stresses exist within the uncoated side of the specimen rather than the coated side. The strain and stress values (including FE) were found to exhibit similar trend. From the experimental strain analysis of the coated disc, we have found that the coating enhances substrate load bearing capability. These results indicate that the variation in plastic strain on coated side is an origin of cracking and it is a cause of delamination during the diametral compression test.

b. Although experimental methods would be deemed most comparable to certain real-life scenario, this type of investigation has its limitations. Locating areas of high stress and analysis through the thickness of the coating are issues when this method is independently used. Before certain conclusions are extrapolated, some additional experimental protocols could be necessary with specimens made from other coating-substrate materials. However, such results provide a simple method to estimate and compare the delamination tendency. This estimation method is useful for optimising the coating adhesion strength.

c. It is possible the proposed methods of analysis were over-simplified. It is known that multiplying strain by the elastic modulus is only correct for the elastic-region of the material, however without knowing official yield points of the coating materials (e.g. $Mo\text{-}Mo_2C/Al_2O_3$) under investigation, this analysis was sufficient for the investigation. The results can be presented further and critically analysed (by including functional coating layer with varied elastic modulus, with additional conclusions being drawn from the numerical modelling.

Acknowledgements

Appendix A

A.1. Supplementary material

Supplementary data (residual strains and stresses) associated with this article can be found in the online version (open access), at https://link.springer.com/article/10.1007/s11340-017-0298-7 [13], and also in **Fig. A.1**.

A.2. Example of analytical stress calculations in disc substrate

As shown in **Table A.2.1**, for a known displacement of compression plate (from experiment), the tensile strength ($\sigma_f = \dfrac{P}{\pi R t} = \dfrac{2P}{\pi D t}$) within a disc in contact with a flat surface can be found. For example, at the centre of the disc surface ($y = R$), as shown in **Fig. 17(a)**, at 1.22 mm displacement with compression load ($P = 19114$ N) for $t_s = 0.00476$ m thick and D $=0.02$ m diameter Hastelloy®X substrate can give tensile stress ($\sigma_f = 127883729$ Pa).

Similarly, the stress ($\sigma_{xs} = \dfrac{P}{\pi}\left\{\dfrac{1}{R} - \dfrac{2\left(a^2 + 2y^2\right)}{a^2\left(a^2 + y^2\right)^{1/2}} + \dfrac{4y}{a^2}\right\}$) within a disc in contact with a flat surface can be found. For example, at the centre of the disc surface ($y = R$), as shown in **Fig. 17(b)**, at 1.22 mm displacement with compression load per unit thickness ($P/t_s = $ 19114/0.00476 = 4015549 N/m) for $t_s = 0.00476$ m thick and $D = 0.02$ m diameter Hastelloy®X substrate can give tensile stress ($\sigma_{xs} = 127632919$ Pa). Where, $a = $ 0.000627528025403582 m, is semi-contact width given by $a^2 = \dfrac{4PR}{\pi E_i^*}$, where $E_i^* = 130$ GPa can be found from composite modulus equation ($\dfrac{1}{E_i^*} = \dfrac{1 - v_1^2}{E_1} + \dfrac{1 - v_s^2}{E_s}$) of the compressing

plate and the disc, R is radius of the disc, and ν_1 and ν_s are Poisson's ratio (**Table A.2.1**) of

non-conformal compressing plates and disc, respectively.

Table A.2.1. Input parameters for analytical calculations.

Parameters	Values
Disc diameter, D (m)	0.02
Disc radius, R (m)	0.01
Disc thickness, t_s (m)	0.00476
Coating thickness, t_c (m)	0.00025
Elastic modulus of Hastelloy®X substrate, E_s (GPa)	269
Poisson's ratio of Hastelloy®X substrate, v_s	0.32
Elastic modulus of Mo-Mo$_2$C/Al$_2$O$_3$ coating surface, E_c (GPa)	147
Poisson's ratio of Mo (for Mo-Mo$_2$C/Al$_2$O$_3$ coating), v_c	0.30
Elastic modulus of compression plate, E_1 (GPa)	210
Poisson's ratio of compression plate, v_1	0.29
Distance of calculation of stresses from contacting plate, $y = R$	0.01

References

[1]   H. Hertz, Über die Berührung fester elastischer Körper (On the Contact of Elastic Solids), Journal für die reine und angewandte. Mathematik. 92 (1881) 156-171.

[2]   K. Johnson, 1985. Normal Contact of Inelastic Solids. In: K. Johnson, ed. Contact Mechanics. Cambridge: Cambridge University Press, 1985, pp. 153-196.

[3]   Y. Jianhong, F.Q. Wu, J.Z. Sun, Estimation of the tensile elastic modulus using Brazilian disc by applying diametrically opposed concentrated loads, International Journal of Rock Mechanics & Mining Sciences. 46 (2009) 568-576.

[4]   S.K. Kourkoulis, Ch.F. Markides, P.E. Chatzistergos, The standardized Brazilian disc test as a contact problem, International Journal of Rock Mechanics & Mining Sciences. 57 (2013) 132-141.

[5]   M. Scapin, L. Peroni, M. Avalle, Dynamic Brazilian test for mechanical characterization of ceramic ballistic protection, Shock and Vibration. Article ID 7485856 (2017) 1-10.

[6]   C. Chen, E. Pan, B. Amadei, Determination of deformability and tensile strength of anisotropic rock using Brazilian tests, Rock Mechanics, 35 (1998) 43-61.

[7]   S.H. Huang, L.S. Lin, A.S. Fok, C.P. Lin, Diametral compression test with composite disk for dentin bond strength measurement – Finite element analysis, Dental Materials. 28 (2012) 1098-1104.

[8]   R. Furukawa, Y. Chen, A. Horiguchi, K. Takagaki, J. Nishi, A. Konishi, Y. Shirakawa, M. Sugimoto, S. Narisawa, Numerical evaluation of the capping tendency of microcrystalline cellulose tablets during a diametrical compression test, International Journal of Pharmaceutics. 493 (2015) 182-191.

[9]   A.T. Procopio, A. Zavaliangos, J.C. Cunningham, Analysis of the diametrical compression test and the applicability to plastically deforming materials, Journal of Materials Science. 38 (2003) 3629-3639.

[10]   M.H. Es-Saheb, A. Albedah, F. Benyahia, Diametral compression test: validation using finite element analysis, The International Journal of Advanced Manufacturing Technology. 57 (2011) 501-509.

[11]   P. Sahoo, B. Chatterjee, A finite element study of elastic-plastic hemispherical contact behavior against a rigid flat under varying modulus of elasticity and sphere radius, Engineering. 2 (2010) 205-211.

[12]   ASTM E9-09, Standard Test Methods of Compression Testing of Metallic Materials at Room Temperature, ASTM International, West Conshohocken, PA, 2009, www.astm.org

[13]   N.H. Faisal, R. Ahmed, A.K. Prathuru, S.P. Katikaneni, M.F.A. Goosen, S.Y. Zhang, Neutron diffraction residual strain measurements of molybdenum carbide based solid oxide fuel cell anode layers with metal oxides on Hastelloy X. Experimental Mechanics. 58 (2018) 585-603.

[14] R. Ahmed, H. Yu, V. Stoica, L. Edwards, J.R. Santisteban, Neutron diffraction residual strain measurements in post-treated thermal spray cermet coatings, Materials Science and Engineering: A. 498 (2008) 191-202.

[15] R. Ahmed, N.H. Faisal, A.M. Paradowska, M. Fitzpatrick, K.A. Khor, Neutron diffraction residual strain measurements in nanostructured hydroxyapatite coatings for orthopaedic implants, Journal of the Mechanical Behavior of Biomedical Materials. 4 (2011) 2043-2054.

[16] R. Ahmed, N.H. Faisal, A.M. Paradowska, M. Fitzpatrick, A comparison of neutron diffraction and hole-drilling residual strain measurements in thermally sprayed coatings, Surface and Coatings Technology. 206 (2012) 4180-4185.

[17] R. Ahmed, N.H. Faisal, A.M. Paradowska, M. Fitzpatrick, Residual strain and fracture response of Al2O3 coatings deposited via APS and HVOF techniques, Journal Thermal Spray Technology. 21 (2012) 23-40.

[18] A.M. Paradowska, A. Tremsin, J.F. Kelleher, S.Y. Zhang, S. Paddea, G. Burca, J.A. James, R. Ahmed, N.H. Faisal, F. Grazzi, G. Festa, C. Andreani, F. Civita, P.J. Bouchard, W. Kockelman, M.E. Fitzpatrick, Modern and historical engineering concerns investigated by neutron diffraction, Journal of Solid Mechanics and Materials Engineering. 6 (2012) 408-418.

[19] C. Godoy, E. A. Souza, M. M. Lima, J. C. A. Batista, Correlation between residual stresses and adhesion of plasma sprayed coatings: effects of a post-annealing treatment. Thin Solid Films. 420-421 (2002) 438–445.

[20] P. Araujo, D. Chicot, M. Staia, J. Lesage, Residual stresses and adhesion of thermal spray coatings. Surface Engineering. 21 (2005) 35-40.

[21] J. Pina, A. Dias, J. L. Lebrun, Study by X-ray diffraction and mechanical analysis of the residual stress generation during thermal spraying. Materials Science and Engineering: A. 347 (2003) 21-31.

[22] S. Sampath, Y. Y. Jiang, J. Matejicek, L. Prchlik, A. Kulkarni, A. Vaidya, Role of thermal spray processing method on the microstructure, residual stress and properties of coatings: an integrated study for Ni–5 wt.%Al bond coats. Materials Science and Engineering: A. 364 (2004) 216–231.

[23] J. Matejicek, S. Sampath, D. Gilmore, R. Neiser, In situ measurement of residual stresses and elastic moduli in thermal sprayed coatings: Part 2: processing effects on properties of Mo coatings. Acta Materialia. 51 (2003) 873-885.

[24] W. Luo, U. Selvadurai, W. Tillman, Effect of residual stress on the wear resistance of thermal spray coating, Journal of Thermal Spray Technology. 25 (2015) (1-2).

[25] N.H. Faisal, R. Ahmed, A.K. Prathuru, S. Spence, M. Hussain, J.A. Steel, An improved Vickers indentation fracture toughness model to assess the quality of thermally sprayed coatings, Engineering Fracture Mechanics. 128 (2014) 189-204.

[26] T. W. Clyne, S. C. Gill, Residual stresses in thermal spray coatings and their effect on interfacial adhesion: A review of recent work. Journal of Thermal Spray Technology. 5 (1996) 401-418.

[27] M. Mellali, P. Fauchais, A. Grimaud, Influence of substrate roughness and temperature on the adhesion/cohesion of alumina coatings. Surface and Coatings Technology. 81 (1996) 275-286.

[28] S. Amada and T. Hirose, Influence of grit blasting pre-treatment on the adhesion strength of plasma sprayed coatings: fractal analysis of roughness. Surface and Coatings Technology. 1998, 102, 132–137.

[29] Y.C. Tsui, C. Doyle, T.W. Clyne, 1998. Plasma sprayed hydroxyapatite coatings on titanium substrates part 1: mechanical properties and residual stress levels. Biomaterials 19 (1998) 2015-2029.

[30] S. Kuroda, T. Dendo, S. Kitahara, Quenching stress in plasma sprayed coatings and its correlation with the deposit microstructure. Journal of Thermal Spray Technology. 4 (1995) 75-84.

[31] S. Timoshenko and J. N. Goodier, Theory of Elasticity. McGrawhill Book Company, Inc. USA, 1951, p. 108.

[32] N.H. Faisal, R. Ahmed, S.P. Katikaneni, S. Souentie, M.F.A. Goosen, Development of plasma sprayed molybdenum carbide-based anode layers with various metal oxide precursors for SOFC, Journal of Thermal Spray Technology. 24 (2015) 1415-1428.

[33] Molybdenum Poisson's ratio; http://www.engineersedge.com/materials/poissons_ratio_metals_materials_chart_13160.htm (accessed 9 January 2016)

[34] Hastelloy® X alloy: Haynes International, Inc., Indiana, USA, 1997.

[35] M. Umemoto, Z.G. Liu, K. Tsuchiya, S. Sugimoto, M.M.A. Bepari, Relationship between hardness and tensile properties in various single structured steels, Materials Science and Technology. 17 (2001) 505-511.

[36] M. Tiryakioğlu, On the relationship between Vickers hardness and yield stress in Al-Zn-Mg-Cu Alloys, Materials Science and Engineering: A. 633 (2015) 17–19.

[37] M. Bäker and P. Seiler, A guide to finite element simulations of thermal barrier coatings, Journal of Thermal Spray Technology. 26 (2017) 1146-1160.

[38] C.H. Hsueh, J.A. Haynes, M.J. Lance, P.F. Becher, M.K. Ferber, E.R. Fuller, S.A. Langer, W.C. Carter, W.R. Cannon, Effects of interface roughness on residual stresses in thermal barrier coatings, Journal of American Ceramic Society. 82 (1999), 1073-1075.

[39] A.D. Jadhav, N.P. Padture, E.H. Jordan, M. Gell, P. Miranzo, Low-thermal-conductivity plasma-sprayed thermal barrier coatings with engineered microstructures, Acta Materialia. 54 (2006), 54, 3343-3349.

[40] P. Michlik and C. Berndt, Image-based extended finite element modeling of thermal barrier coatings, Surface and Coatings Technology. 201 (2006) 2369-2380.

[41] N. Nayebpashaee, S. Seyedein, M. Aboutalebi, H. Sarpoolaky, S. Hadavi, Finite element simulation of residual stress and failure mechanism in plasma sprayed thermal

barrier coatings using actual microstructure as the representative volume, Surface and Coatings Technology. 291 (2016) 103-114.

[42]   A.M. Kamara and K. Davey, A numerical and experimental investigation into residual stress in thermally sprayed coatings, International Journal of Solids and Structures. 44 (2007) 8532-8555.

[43]   ASTM C633-13(2017), Standard Test Method for Adhesion or Cohesion Strength of Thermal Spray Coatings, ASTM International, West Conshohocken, PA, 2017, www.astm.org.

[44]   M. Mellor, I. Hawke, Measurement of tensile strength by diametral compression of discs and annuli, Engineering Geology, 5 (1971) 173-225.

[45]   W.S. Sampath, T.C. Ramaraj, M.C. Shaw, A crack detection technique for use with brittle materials. Journal of Engineering for Industry. 108 (1986) 232-235.

[46]   Y.C. Tsui, T.W. Clyne, An analytical model for predicting residual stresses in progressively deposited coatings Part 1: Planar geometry. Thin Solid Films 306 (1997) 23-33.

Figure Captions

Figure 1. Diametrical compression testing method (Brazilian test): (a) before loading, (b) after loading, and (c) theoretical considerations during loading.

Figure 2. Test set-up for diametral compression (Brazilian test) showing the side view: (a) substrate only, and (b) substrate with coating.

Figure 3. (a) Thermally spray coating specimen (Mo-Mo_2C/Al_2O_3 coating on Hastelloy-X$^®$ substrate), and (b) diametral compression test assembly on disc specimen.

Figure 4. Elastic modulus through thickness (measured using diamond Berkovich nanoindentation method at 30 mN load at room temperature, using NanoTest^{TM} system) [inbox shows the scheme of indentation array at the coating-substrate cross-section].

Figure 5. Finite element model set-up in ABAQUS (v.6.16) of Hastelloy$^®$X substrate with the Mo-Mo_2C/Al_2O_3 coated on one surface: (a) loading and boundary conditions defined for the model, and (b) converged mesh for the model consisting of 28,392 elements for substrate and 2366 elements for the coating.

Figure 6. Diametrical compression testing on standalone Hastelloy-X® substrate during loading showing strain and stress within the centre of the specimen: (a) surface x- and y-axis strain, and (b) surface x- and y-axis stress [leftward arrow locations in both figures shows the location of final strain or stress].

Figure 7. Diametrical compression testing during loading showing stresses at the centre of the Mo-Mo$_2$C/Al$_2$O$_3$ coated specimen (alumina): (a) strains, and (b) stresses, and (c) normalised stresses (for substrate uncoated side).

Figure 8. SEM images of Mo-Mo$_2$C/Al$_2$O$_3$ coated specimen: (a) coated surface, and (b) cross-section surface.

Figure 9. Comparison of diametrical compression testing during loading showing stresses at each material surface: (a) strain, (b) stress, and (c) normalised stress.

Figure 10. Diametral compression tested specimens (Mo-Mo$_2$C/Al$_2$O$_3$ coated on Hastelloy®X substrate): (a) before peeling (after compression test), and (b) substrate (after compression test, manual peeling of coating) showing two distinct delamination features symmetric on both side of the vertical axis.

Figure 11. Equivalent von-Mises stress (MPa) acting on the substrate and coating for the diametric compression test simulated using ABAQUS (elastic-plastic model): (a) von-Mises stress for the substrate on the coated face, (b) von-Mises stress acting on the substrate on the uncoated face, (c) von-Mises stress acting on the coating for the non-interacting surface with the substrate, and (d) von-Mises stress acting on the coating for the interacting surface with the substrate.

Figure 12. Shear stress (MPa) acting on the XY plane for the coating and substrate simulated using ABAQUS (elastic-plastic model): (a) XY shear stress for the substrate on the coated face, (b) XY shear stress acting on the substrate on the uncoated face, (c) XY shear stress for the coating for the non-interacting surface, and (d) XY shear stress for the coating for the interacting surface.

Figure 13: Variation of finite element stresses at the centre of the Mo-Mo$_2$C/Al$_2$O$_3$ coating and Hastelloy$^®$X substrate: (a) for elastic-plastic model, and (b) perfectly elastic model.

Figure 14. The path in the disc specimen along which the graphs have been plotted in ABAQUS for the von-Mises and XY shear stress of the coating and substrate (Path-1 for von-Mises stress along Y-direction, Path-2 for von-Mises stress along X-direction, Path-3 for XY shear stress (right orientation), and Path-4 for XY shear stress (left orientation)).

Figure 15. The von-Mises stress (elastic-plastic model) on the Mo-Mo$_2$C/Al$_2$O$_3$ coating and Hastelloy$^®$X substrate for surface interacting with the each other: (a) along the x-axis, and (b) along the y-axis. The shaded area in both plots indicates the mismatch of stress at the coating-substrate interface.

Figure 16. XY shear stress (elastic-plastic model) acting on the Mo-Mo$_2$C/Al$_2$O$_3$ coating and Hastelloy$^®$X substrate for surface interacting with the each other: (a) right orientation in substrate with left orientation in coating, and (b) left orientation in substrate with right orientation in coating. The shaded area in both plots indicates the mismatch of stress at the coating-substrate interface.

Figure 17. Analytical calculations: Comparison of diametrical compression testing during loading showing stresses at each material disc centre (at y = R): (a) bi-axial x- and y-direction stresses using Eqs. (10a,b), (b) x-direction stresses (using Eqs. (11a, 12a)), and (c) y-direction stresses (using Eqs. (11b, 12b)).

Fig. A.1. Neutron diffraction measurements and comparison (based on average of all individual peak routine analysis) of thermally spray coating specimen (250 µm thick Mo-Mo$_2$C/Al$_2$O$_3$ coating on 4.76 mm thick Hastelloy-X$^®$ substrate): (a) residual strain, and (b) corresponding residual stress.
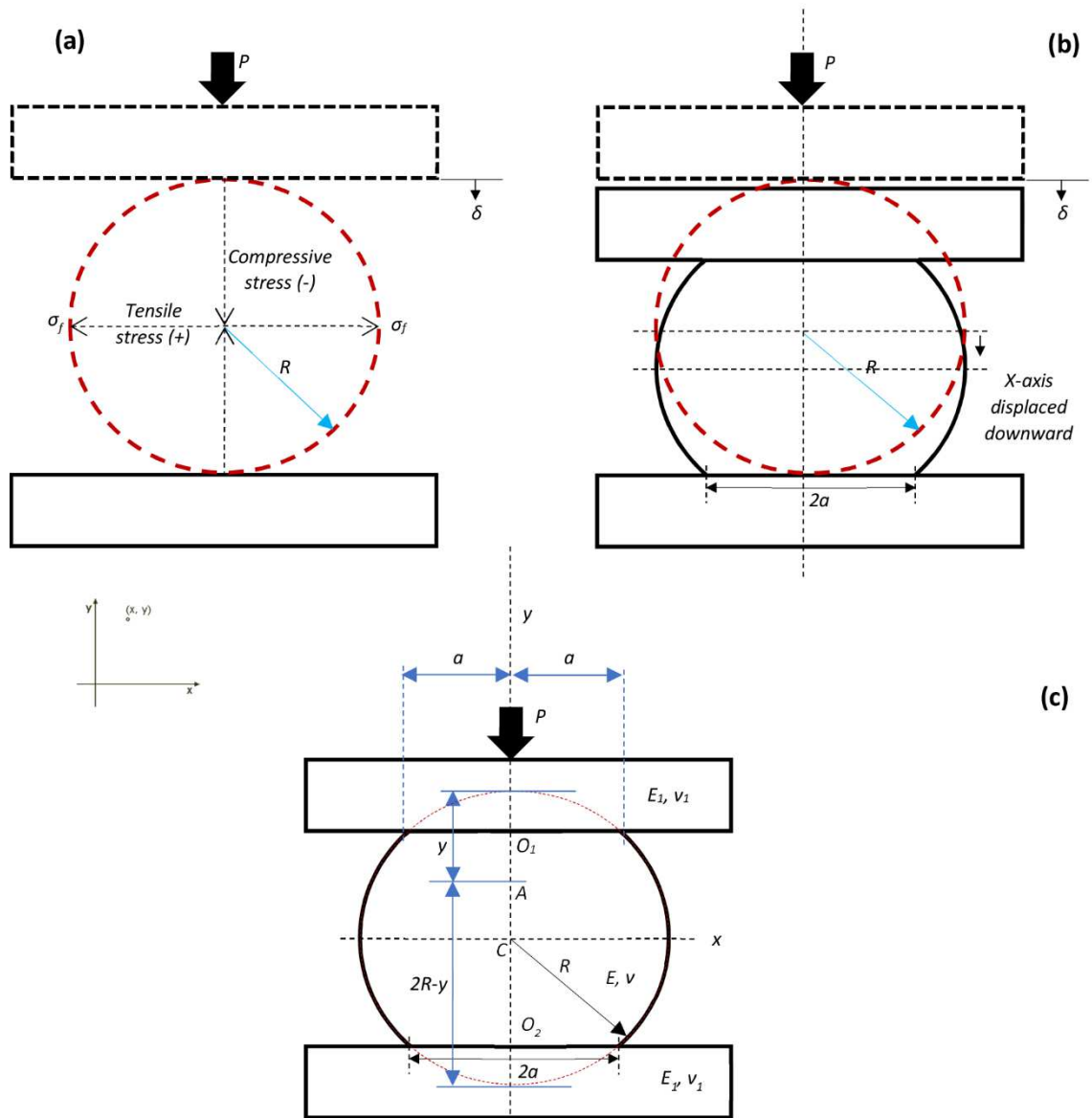
Figure 1
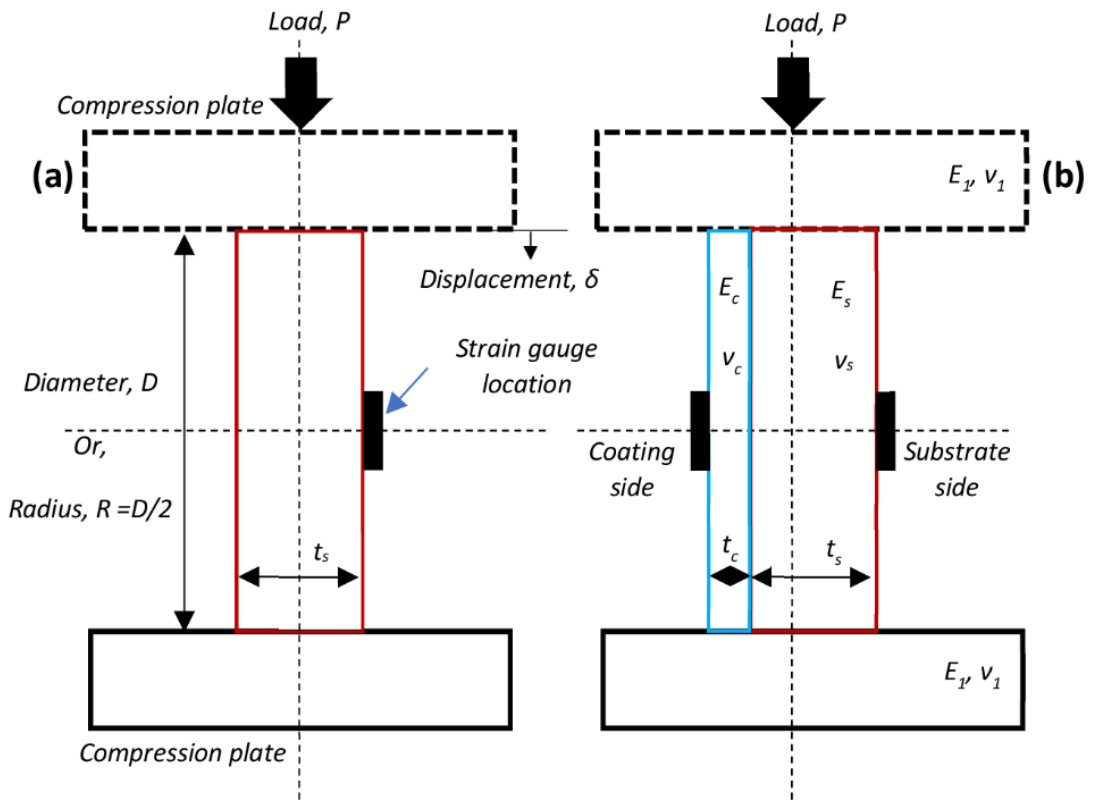
Substrate diameter, D = 20 mm; Substrate thickness, t_s = 4.76 mm
Coating thickness, t_c = 0.25 mm; Displacement, δ = 1.6 mm
Plate height = 5 mm, Plate length = 20 mm, Plate thickness = 10 mm
E_s = 269 GPa, v_s = 0.32, E_c = 147 GPa (surface), v_s = 0.30
E_1 = 210 GPa, v_1 = 0.29

Figure 2

(a)

Mo-Mo₂C/Al₂O₃ coating

Coating residue around the disc edge

Hastelloy®X disc substrate

(b)

Test assembly

Notched Plastic Jig

Test Specimen

Strain Gauge Rosette
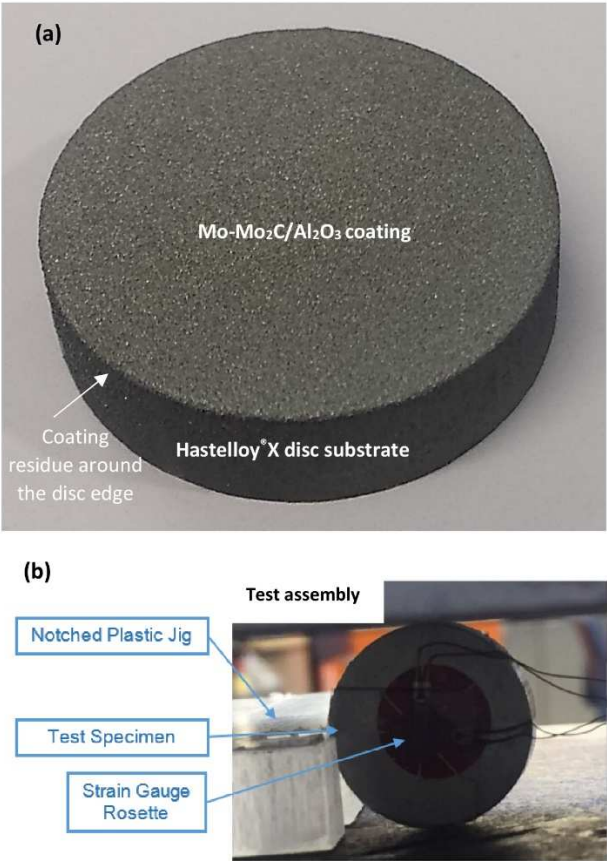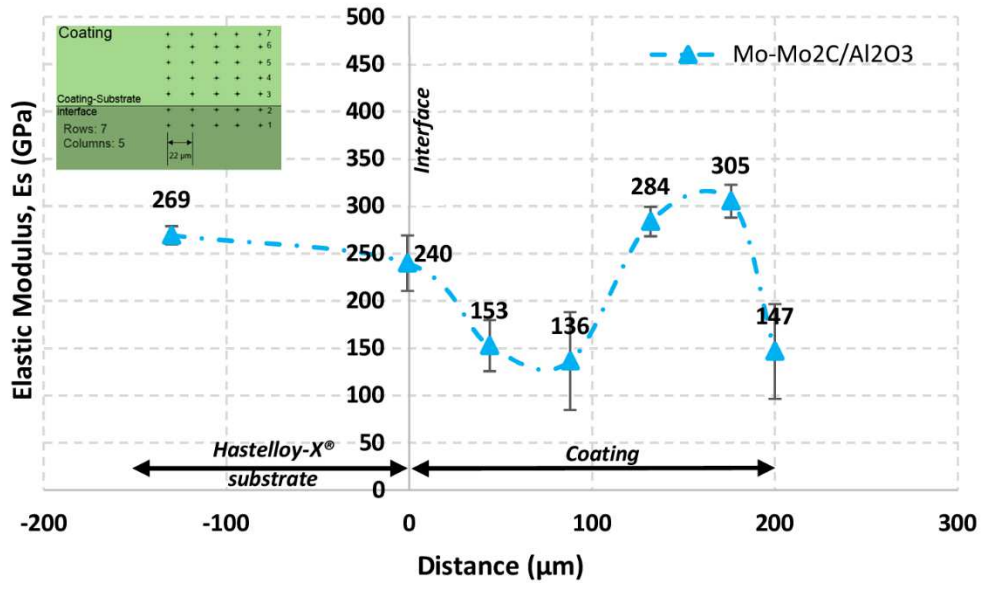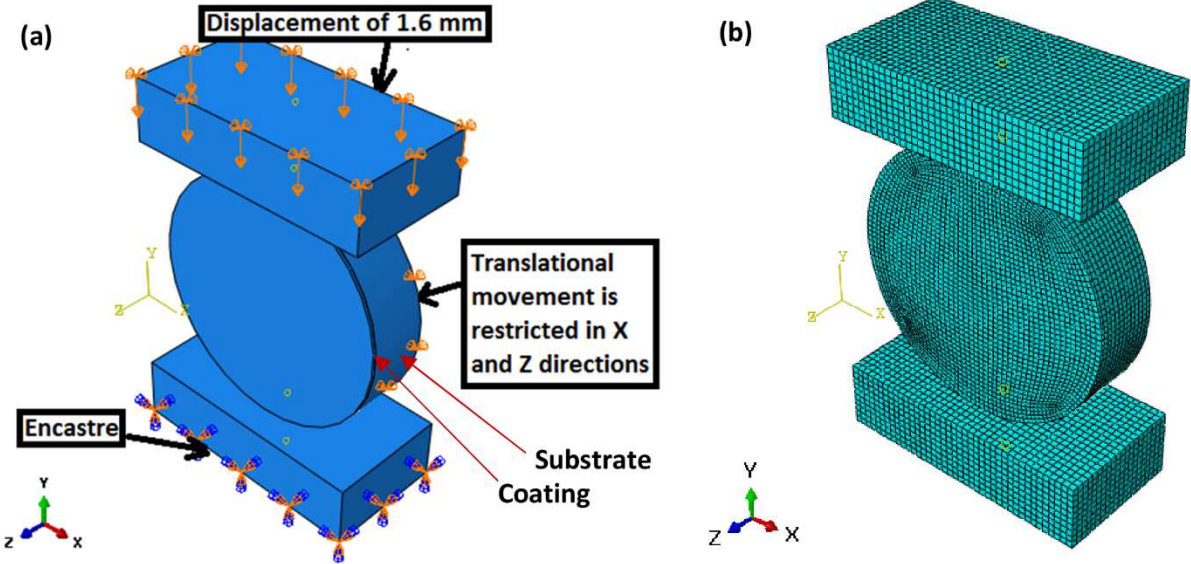
Figure 3

Figure 4

Figure 5
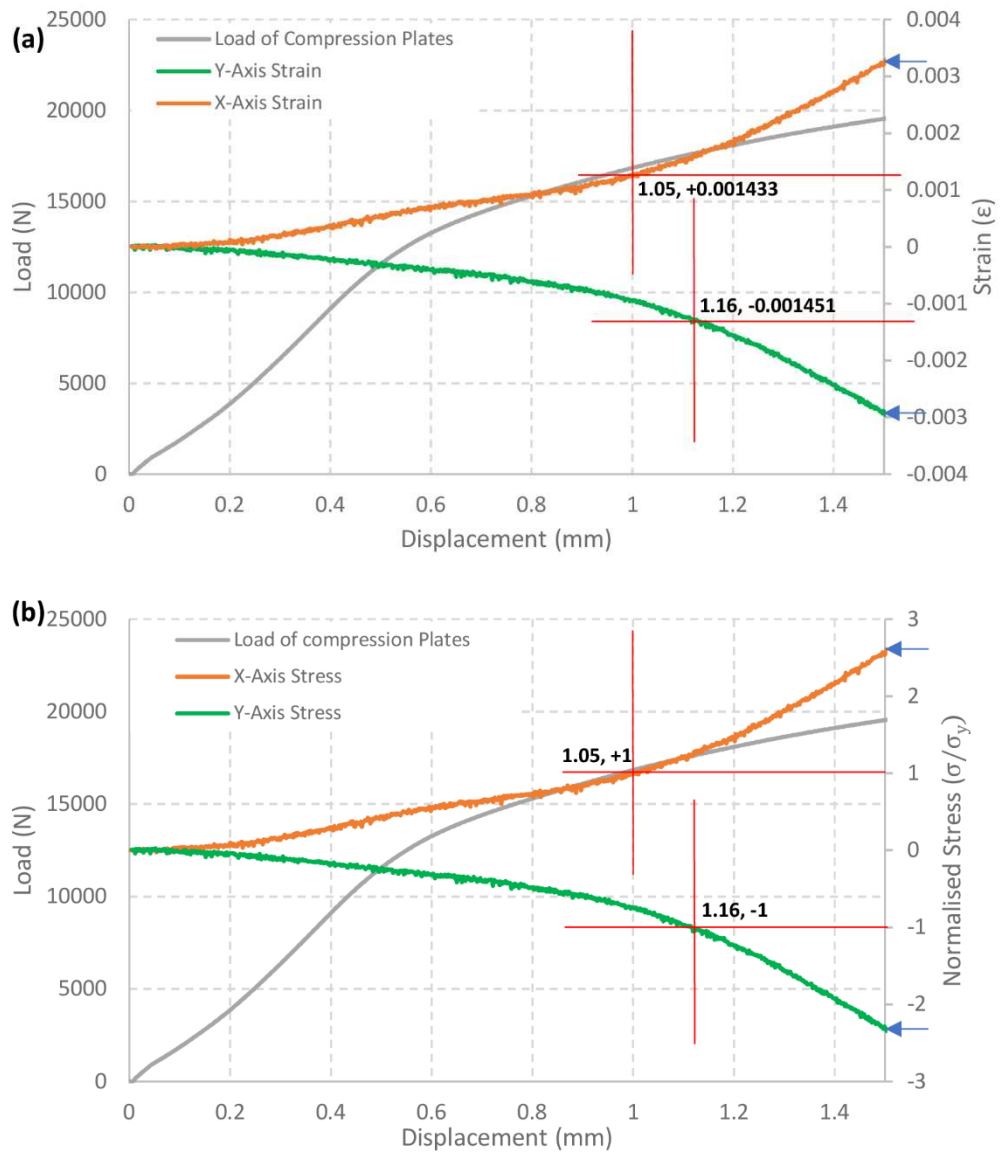
Figure 6
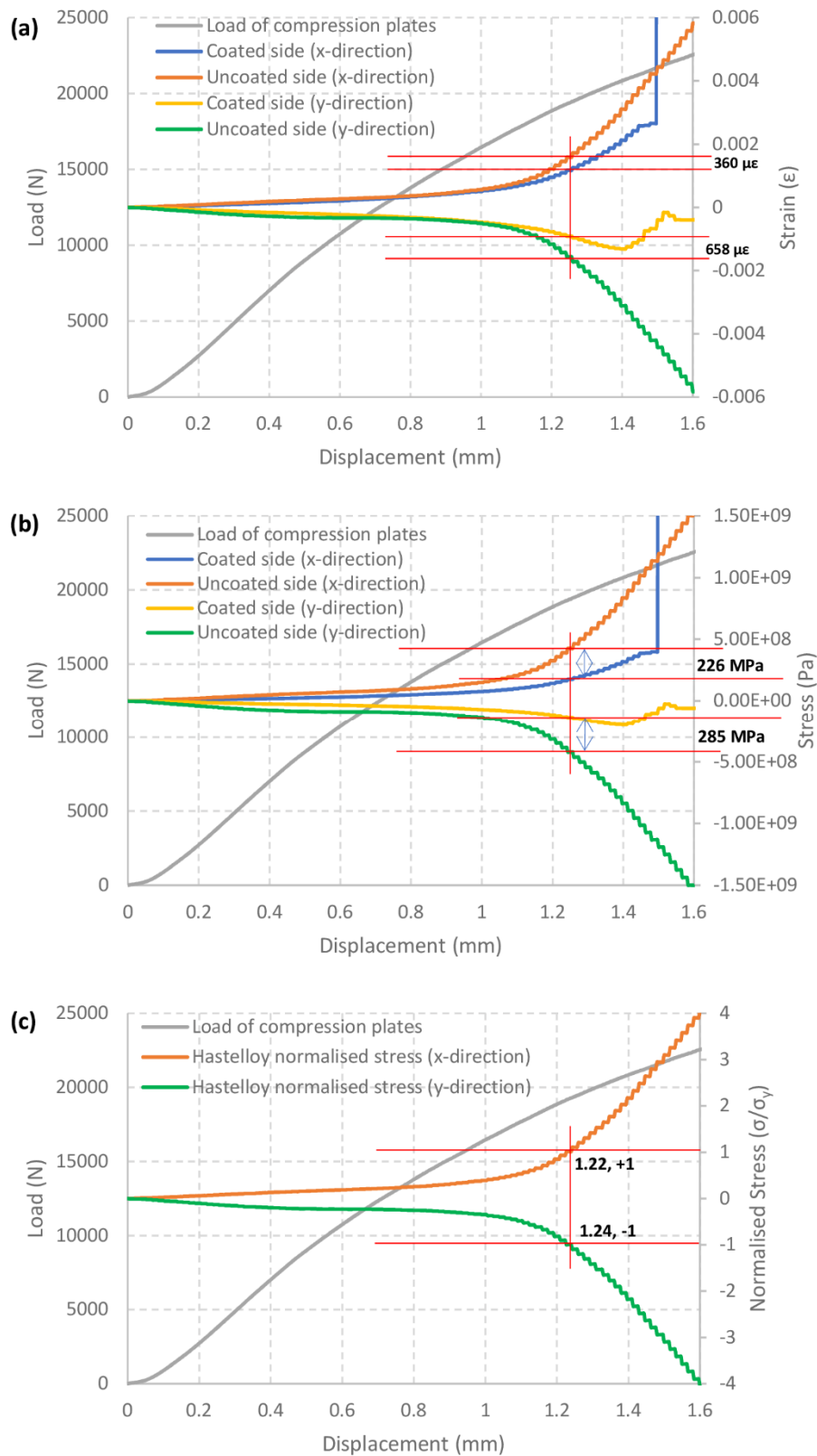
Figure 7
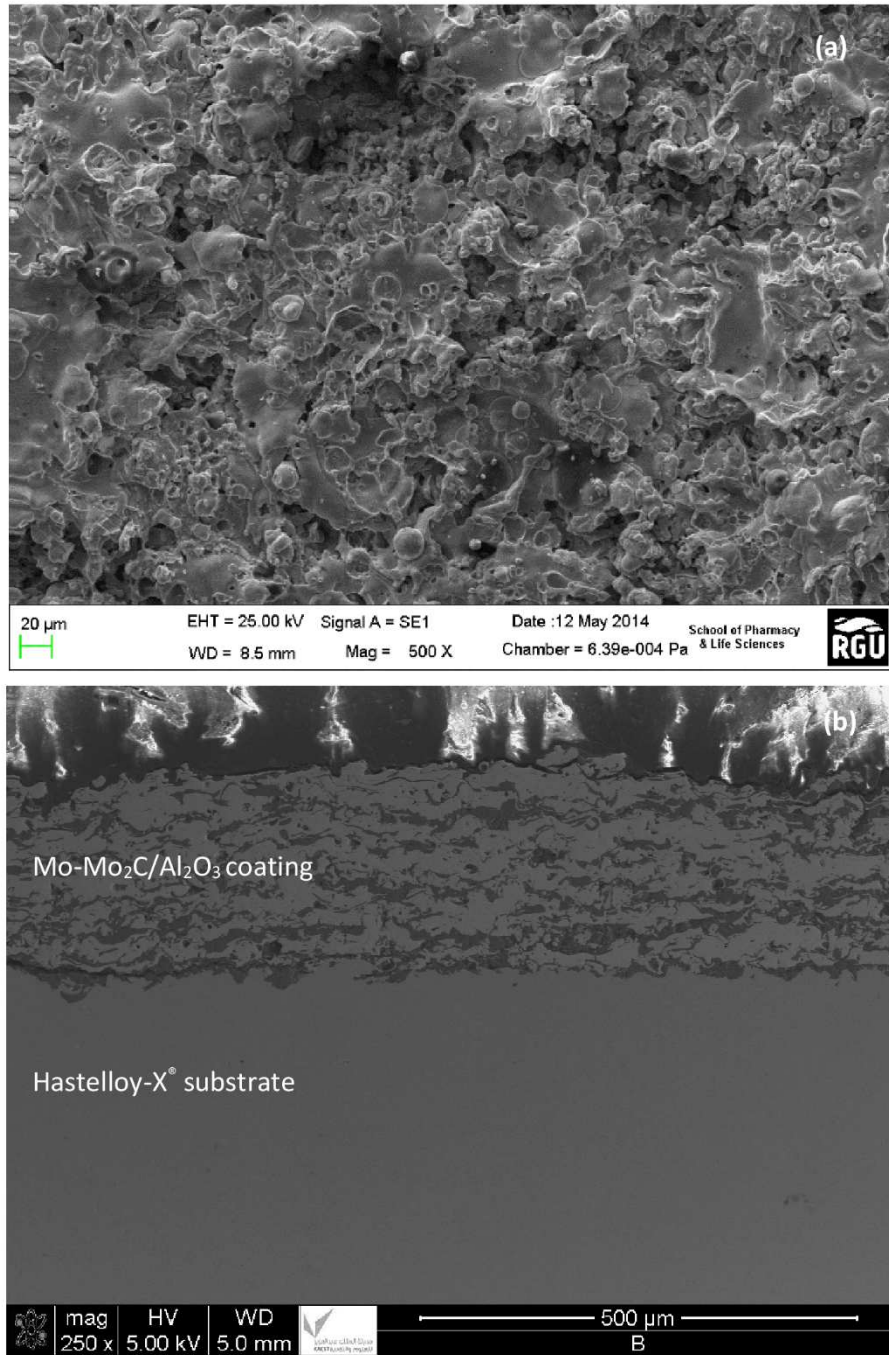
*Figure 8*
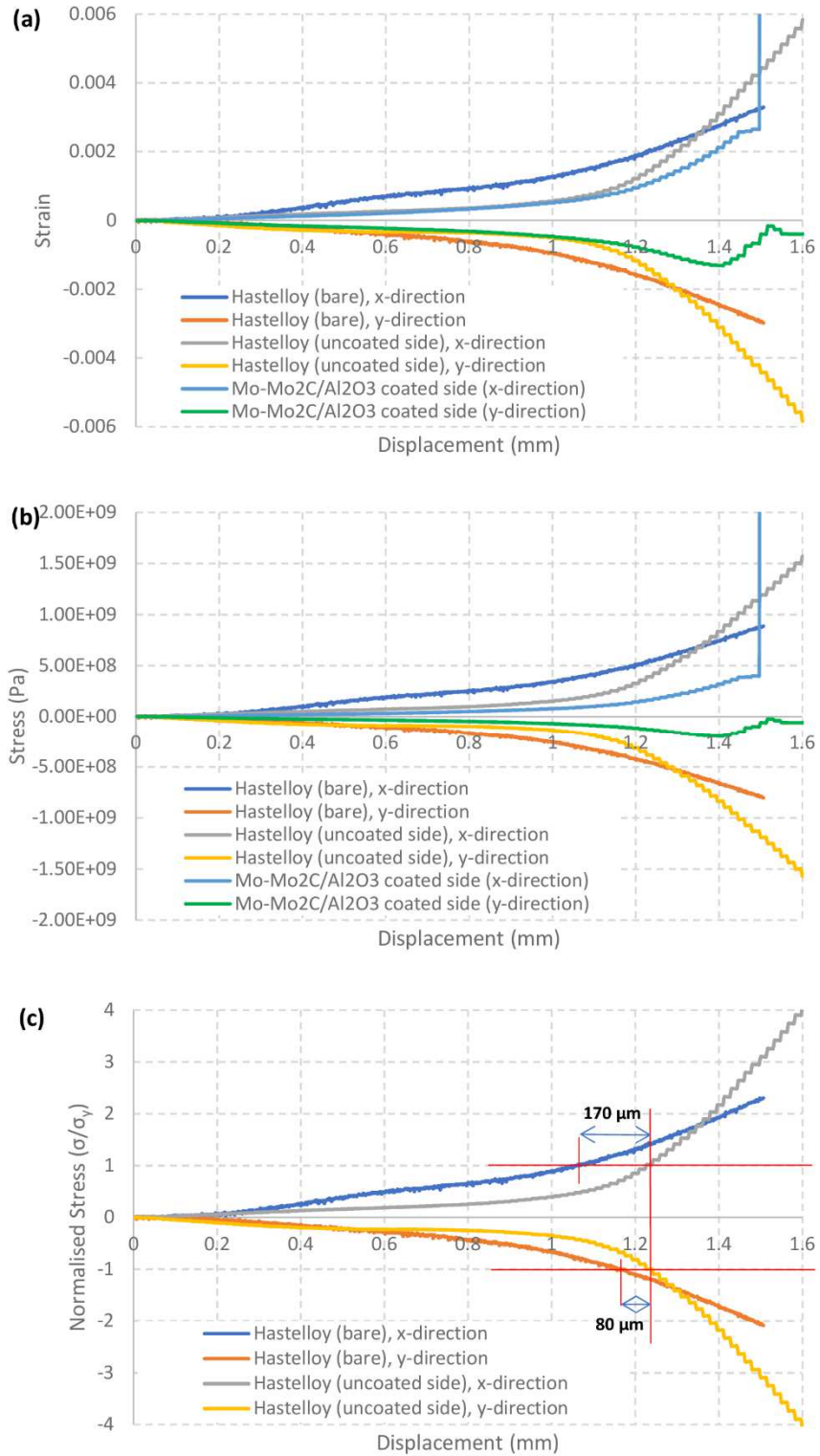
Figure 9
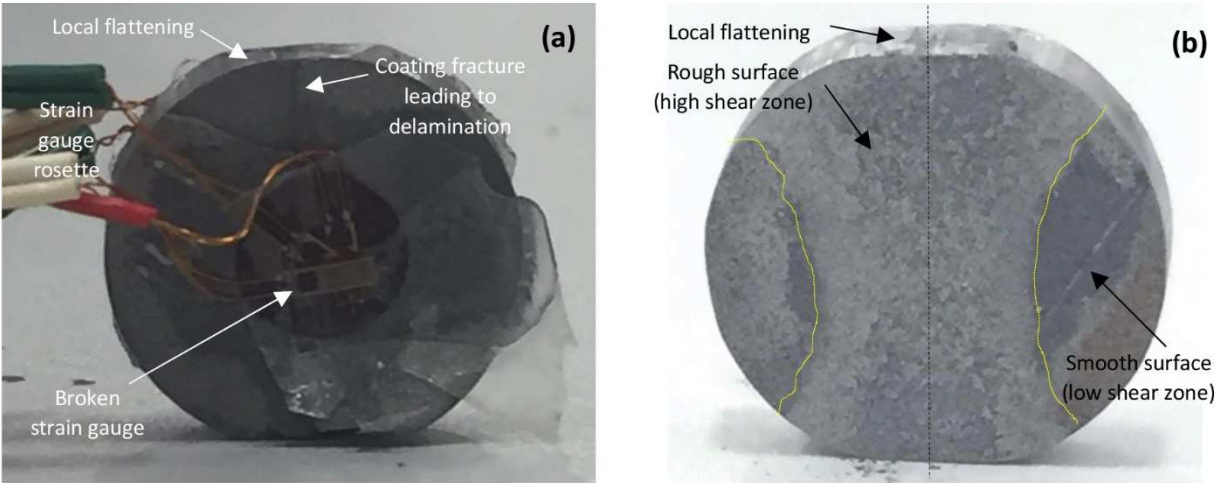
Figure 10
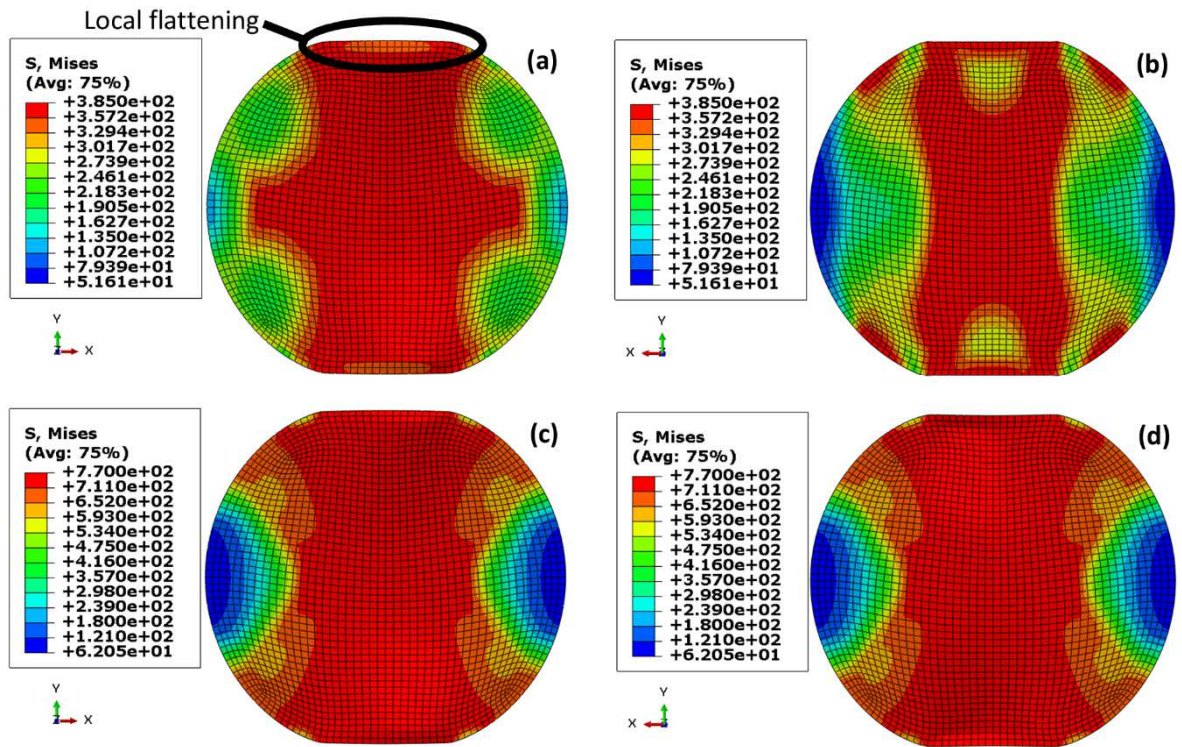
Figure 11
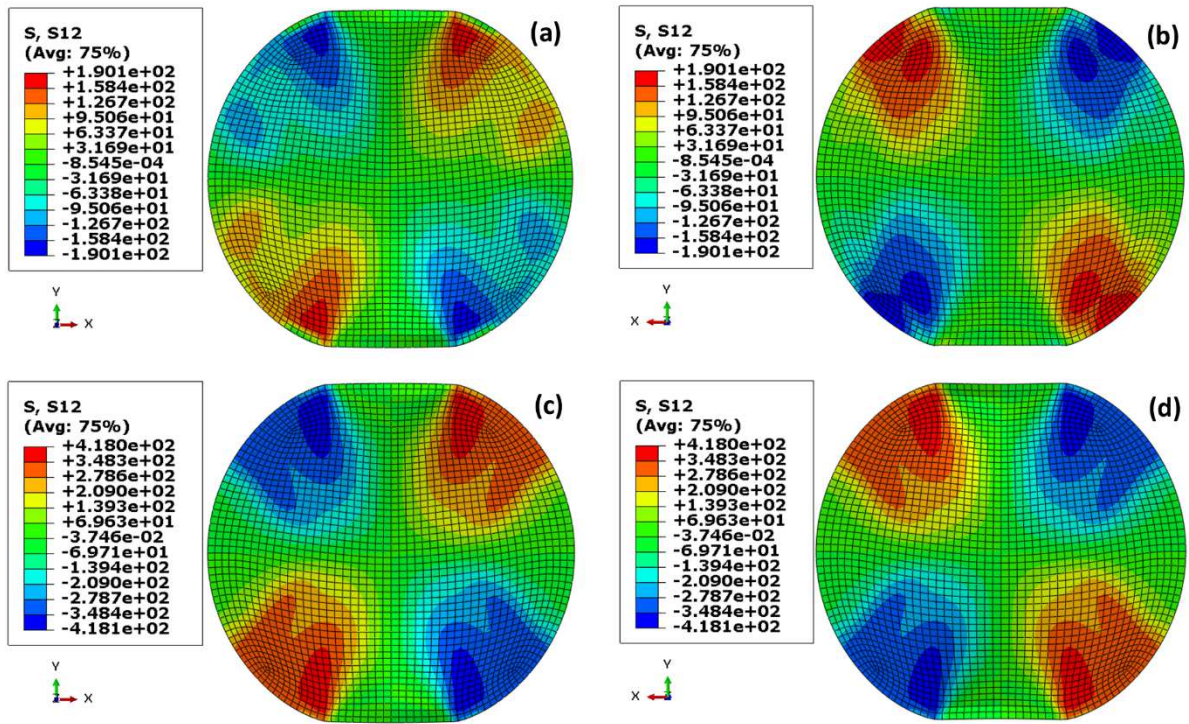
Figure 12
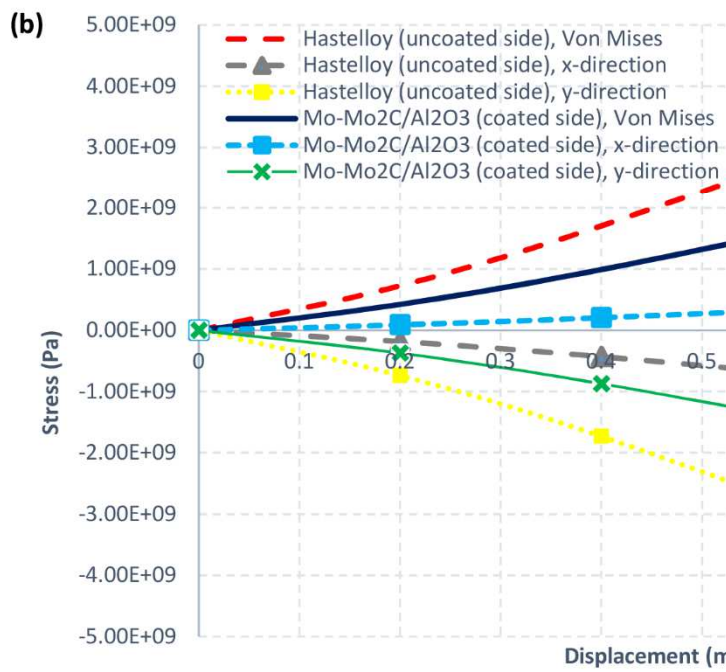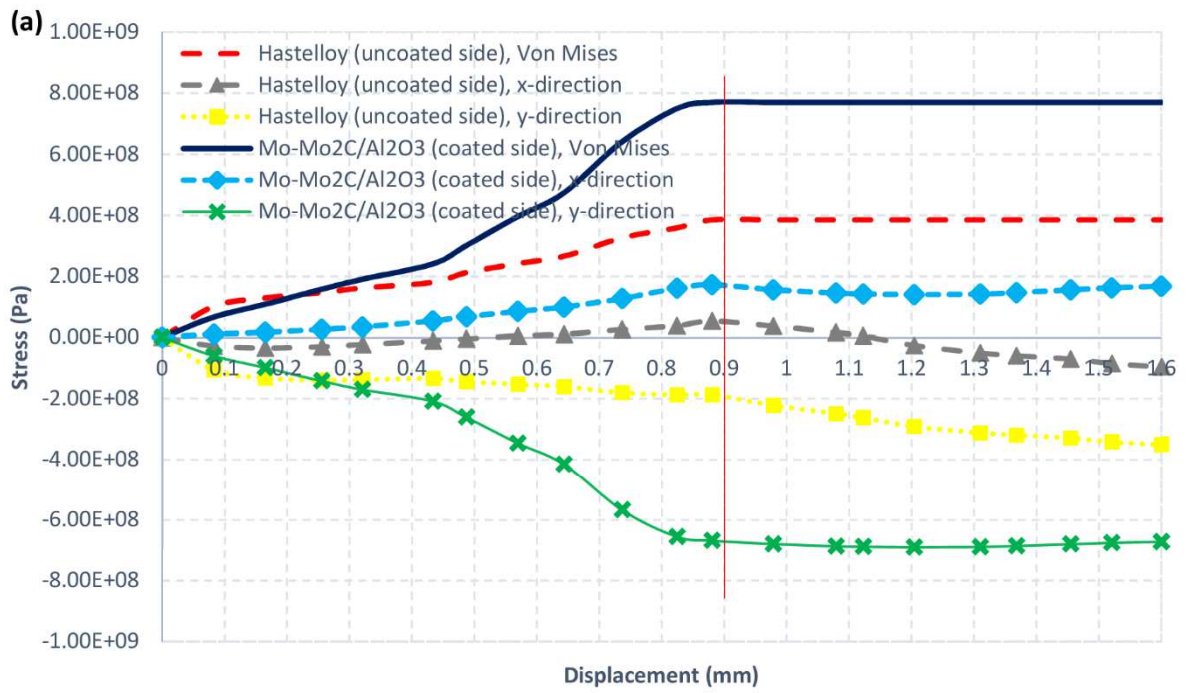
Figure 13
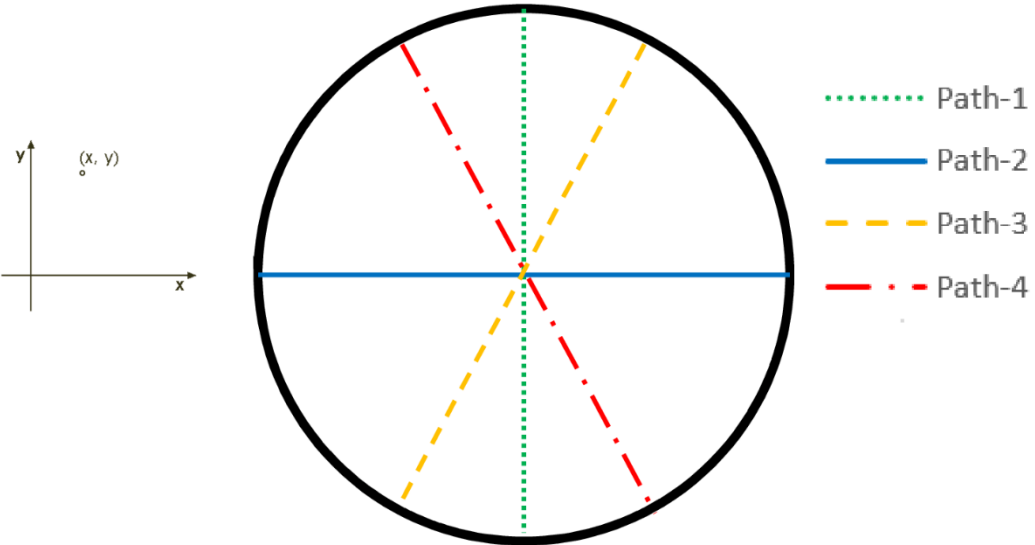
Figure 14
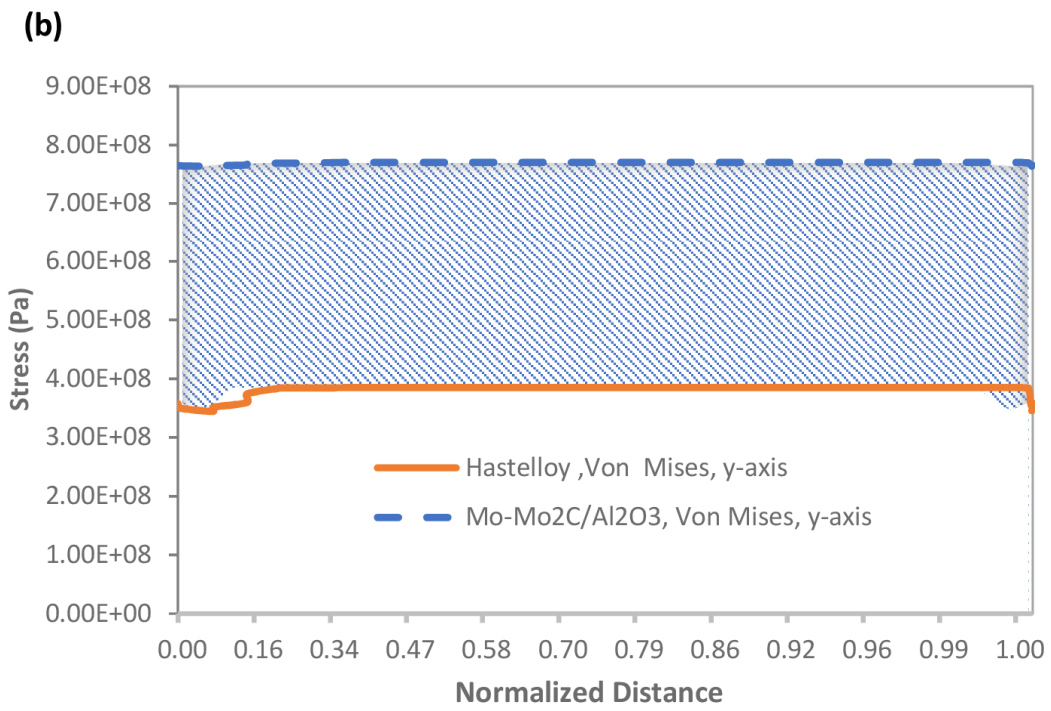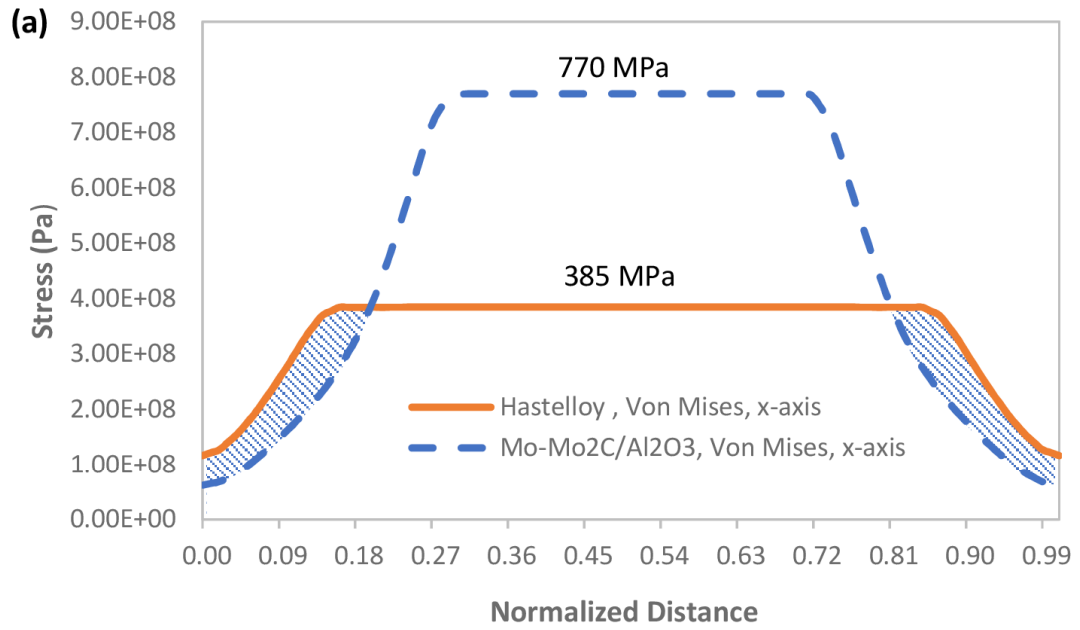
Figure 15
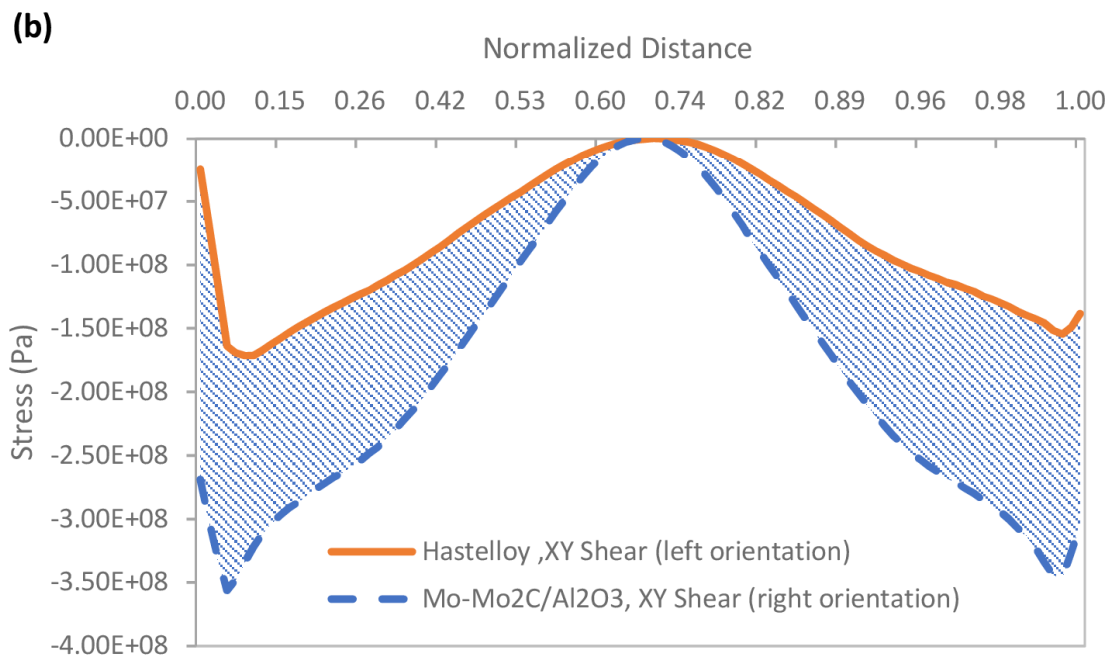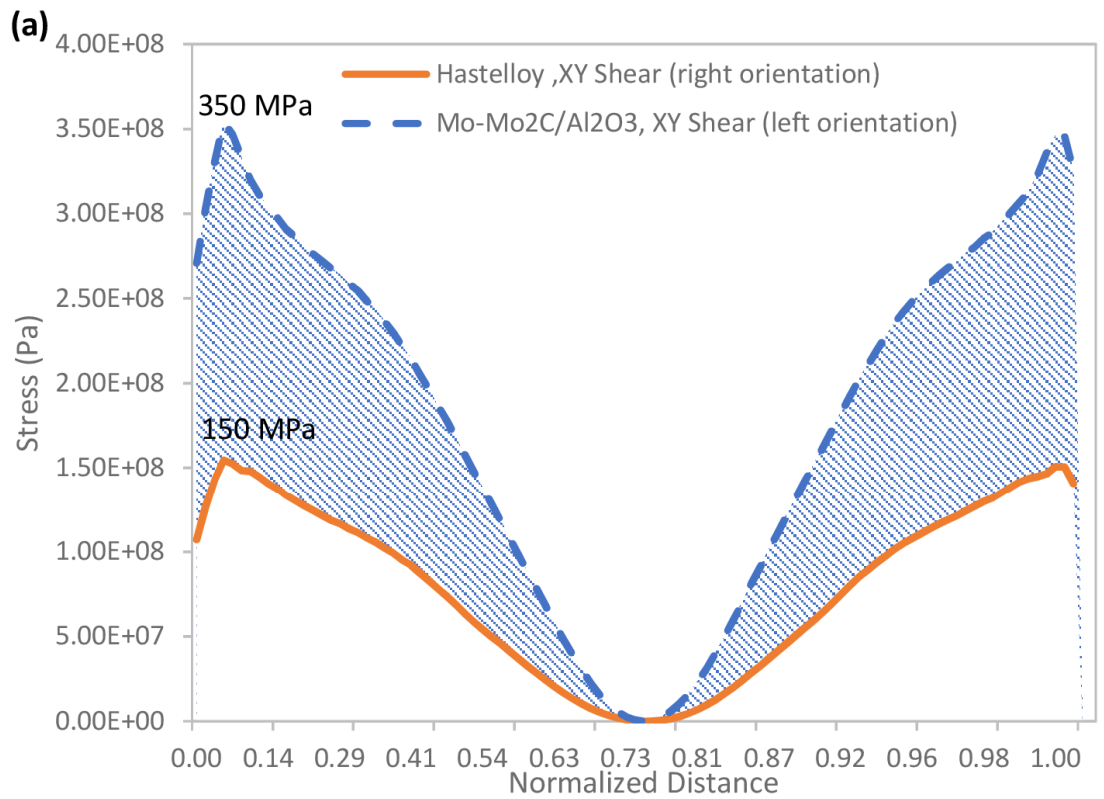
Figure 16

Figure 17

Figure A.1